Design, synthesis and biological evaluation of PD-1 derived peptides as inhibitors of PD-1/PD-L1 complex formation for cancer therapy

Bioorganic Chemistry 128 (2022) 106047

Contents lists available at ScienceDirect

Bioorganic Chemistry

journal homepage: www.elsevier.com/locate/bioorg

Design, synthesis and biological evaluation of PD-1 derived peptides as inhibitors of PD-1/PD-L1 complex formation for cancer therapy

Magdalena Bojko [a], Katarzyna Węgrzyn [b], Emilia Sikorska [a], Mikołaj Kocikowski [c], Maciej Parys [d], Claire Battin [e], Peter Steinberger [e], Małgorzata M. Kogut [a], Michał Winnicki [a], Adam K. Sieradzan [a], Marta Spodzieja [a,*], Sylwia Rodziewicz-Motowidło [a,*]

[a] Faculty of Chemistry, University of Gdańsk, 80-308 Gdańsk, Poland
[b] Intercollegiate Faculty of Biotechnology UG&MUG, University of Gdańsk, 80-307 Gdańsk, Poland
[c] International Centre for Cancer Vaccine Science, University of Gdańsk, 80-822 Gdańsk, Poland
[d] The Royal (Dick) School of Veterinary Studies and The Roslin Institute, University of Edinburgh, Easter Bush Campus, Midlothian EH25 9RG, United Kingdom
[e] Division of Immune Receptors and T Cell Activation, Institute of Immunology, Medical University of Vienna, 1090 Vienna, Austria

ARTICLE INFO

Keywords:
Programmed cell death 1 protein (PD-1)
Programmed cell death ligand 1 protein (PD-L1)
Immune checkpoint inhibitor
Disulfide-linked peptide
Immunotherapy
NMR conformational studies
Molecular docking
Surface plasmon resonance
Bioluminescence blockade assay
Stability of peptides

ABSTRACT

Over the past few years, many molecules such as monoclonal antibodies, affibodies, nanobodies, and small compounds have been designed and tested as inhibitors of PD-1/PD-L1 complex formation. Some of them have been successfully implemented into clinical oncology practice. However, the majority of these compounds have disadvantages and limitations, such as high production price, potential for immunogenicity and/or prolonged clearance. Thus, new inhibitors of the PD-1/PD-L1 immune checkpoints are needed. Recently, peptides emerged as potential novel approach for blocking receptor/ligand interaction. In the presented studies we have designed, synthesised and tested peptides, which are potential inhibitors of the PD-1/PD-L1 axis. The amino acid sequences of the designed peptides were based on the binding sites of PD-1 to PD-L1, as determined by the crystal structure of the protein complex and also based on MM/GBSA analysis. Interactions of the peptides with PD-L1 protein were confirmed using SPR, while their inhibitory properties were studied using cell-based PD-1/PD-L1 immune checkpoint blockade assays. The characterization of the peptides has shown that the peptides PD-1(119–142)$^{T120C\text{-}E141C}$, PD-1(119–142)$^{C123\text{-}S137C}$ and PD-1(122–138)$^{C123\text{-}S137C}$ strongly bind to PD-L1 protein and disrupt the interaction of the proteins. PD-1(122–138)$^{C123\text{-}S137C}$ peptide was shown to have the best inhibitory potential from the panel of peptides. Its 3D NMR structure was determined and the binding site to PD-L1 was established using molecular modelling methods. Our results indicate that the PD-1 derived peptides are able to mimic the PD-1 protein and inhibit PD-1/PD-L1 complex formation.

Abbreviations: **Abu**, 2-aminobutyric acid; **ANOVA**, one-way analysis of variance; **APC**, antigen-presenting cell; **ATP**, adenosine triphosphate; **CHO**, Chinese hamster ovary; **DSS**, sodium trimethylsilylpropanesulfonate; **EC_{50}**, half maximal effective concentration; **FBS**, fetal bovine serum; **FDA**, Food and Drug Administration; **gMFI**, geometric mean of fluorescence intensity; **HSQC**, heteronuclear single quantum correlation; **HTRF**, homogeneous time resolved fluorescence; **IgSF**, immunoglobulin superfamily; **IgC2**, immunoglobulin constant type2 domain; **IgV**, immunoglobulin variable domain; **K_D**, equilibrium dissociation constant; **LC ESI-IT-TOF MS**, liquid chromatography coupled with electrospray ionization, ion trap, and time-of-flight mass spectroscopy; **mAb**, monoclonal antibody; **irAEs**, immune-related adverse events; **MD**, molecular dynamics; **MM/GBSA**, molecular mechanics generalized Born surface area; **MM/PBSA**, molecular mechanics Poisson–Boltzmann surface area; **MREMD**, multiplexed-replica exchange molecular dynamics; **NFAT**, nuclear factor of activated T cells; **NFAT-RE**, nuclear factor of activated T cells response element; **NMR**, nuclear magnetic resonance; **NOE**, nuclear Overhauser effect; **NOESY**, nuclear Overhauser effect spectroscopy; **PD-1**, programmed cell death 1; **PDB**, protein data bank; **PD-L1**, programmed cell death-ligand 1; **PD-L2**, programmed cell death-ligand 2; **RLU**, relative luminescence units; **RMSD**, root-mean-square deviation; **ROESY**, rotating frame Overhauser effect spectroscopy; **RP-HPLC**, reversed phase-high performance liquid chromatography; **RPMI 1640**, Roswell Park Memorial Institute 1640 medium; **RU**, resonance units; **SD**, standard deviation; **SPR**, surface plasmon resonance; **TCS**, T cell stimulator cells; **TOSCY**, total correlation spectroscopy; **UNRES**, UNited RESidue; **WHAM**, weighted histogram analysis method.

* Corresponding authors.
E-mail addresses: marta.spodzieja@ug.edu.pl (M. Spodzieja), s.rodziewicz-motowidlo@ug.edu.pl (S. Rodziewicz-Motowidło).

https://doi.org/10.1016/j.bioorg.2022.106047
Received 12 April 2022; Received in revised form 4 July 2022; Accepted 19 July 2022
Available online 22 July 2022

1. Introduction

The idea of blocking PD-1/PD-L1 complex to treat cancer has its beginnings in the early 2000′s [1]. In 2014 the first anti-PD-1 monoclonal antibodies (mAbs) pembrolizumab [2] and nivolumab [3] were approved by the Food and Drug Administration (FDA) for the treatment of melanoma, non-small-cell lung cancer and Hodgkin's lymphoma [4]. Since then, several other anti-PD-1 and anti-PD-L1 mAbs have obtained approval, including cemiplimab, atezolizumab, avelumab and durvalumab [5–8]. Apart from the aforementioned mAbs, in the current year alone, there are more than one thousand ongoing trials with single agents and combinatory approaches that target PD-1 or PD-L1 proteins [9,10].

Programmed cell death 1 protein (PD-1, CD279) is an immune checkpoint receptor belonging to the immunoglobulin superfamily (IgSF). It consists of 288 amino acids divided into: a signal peptide, an extracellular immunoglobulin variable (IgV)-like domain, and transmembrane and cytoplasmic domains [11]. PD-1 has four potential *N*-linked glycosylation sites in the IgV domain [12]. PD-1 is expressed in small amounts on naïve T cells and on activated T and B cells, dendritic cells, monocytes, and natural killer T cells [11,13]. It has two naturally occurring ligands, namely PD-L1 and PD-L2 [14]. Both these ligands bind to the IgV domain of the receptor, which is also responsible for signal transduction to intracellular domains. Upon interaction with PD-L1 PD-1 induces intracellular signalling pathways that result in the inhibition of T lymphocyte proliferation, cytokine production, and cytolytic function [15]. The role of PD-L2 in regulation of T cell responses is controversial as both inhibitory and stimulatory functions have been described [16–18].

PD-L1 (B7-H1, CD274) and PD-L2 (B7-DC, CD273) also belong to the IgSF and they have structures similar to the PD-1 receptor but each of them contains, in the extracellular part, IgV and immunoglobulin constant type2 (IgC2) domains connected by a short linker. The *N*-terminal IgV domain of each ligand is responsible for binding to the PD-1 receptor. The role of the *C*-terminal domain is unknown. PD-L1 is broadly expressed on cells of the hematopoietic lineage including activated T cells [19]. Inflammatory stimuli induce PD-L1 expression and it is also expressed in a wide variety of non-hematopoietic tissues [20,21]. Moreover, PD-L1 can be expressed in many types of tumours, including melanoma, non-small-cell lung cancer, breast and bladder cancer, Hodgkin's lymphoma, and renal cell carcinoma [22,23]. PD-L2 is expressed on activated dendritic cells, mast cells and macrophages [16,17] and additionally, it is also expressed on cancer cells [24]. The affinity of PD-1 to its ligands is in the low micromolar range [14]. The value of the equilibrium dissociation constant (K_D) of the PD-1/PD-L1 complex differs depending on the analytical method and is estimated at between 1.15 and 8.2 μM. For the PD-1/PD-L2 interaction this value is 2.6 μM [25–28].

The first human PD-1/PD-L1 complex structure (PDB code: 4ZQK) was obtained by Zak et al. in 2015 [29]. The receptor and ligand form a complex in a 1:1 stoichiometry [25,29,30]. Two fragments of PD-1 in the middle part of protein (amino acids in positions: Y68, Q75, T76, K78) and in the *C*-terminus (A132, I134, E136) interact with three PD-L1 fragments. The following amino acids from PD-L1 are crucial for the interaction with the receptor: A19, F26, Y56, E58, Q66, R113, A121, D122, Y123, K124, and R125. Since the crystal structure of the PD-1/PD-L1 complex was obtained, numerous studies have been carried out to design peptides which are potential inhibitors of the proteins' interaction and are based on PD-1 or PD-L1 binding interface [31–33]. In 2019 the crystal structure of human PD-1/PD-L2 (PDB code: 6UMT) was also determined and it may be used to design compounds which disrupt this interaction [14].

There are many approaches used to the design of peptides targeting protein/protein interactions, including molecular modelling, rational design, hot spot theory, or phage display technology [34,35]. Previously published studies described linear, branched and cyclic peptides targeting PD-1 or PD-L1 protein [31]. Nonetheless, none of these has reached clinical trials up to now. The first peptidomimetic reaching phase I clinical research is CA-170, which is descended from AUNP-12 peptide and is produced by the Aurigene company. It exhibits a half maximal effective concentration (EC_{50}) value of 17 nM [36,37]. However, data published by Musielak et al. did not confirm its ability to interact with PD-L1 protein as shown by various assays such as homogeneous time resolved fluorescence (HTRF), nuclear magnetic resonance (NMR) binding assay, and cell-based PD-1/PD-L1 inhibition assay [38]. These results indicate, that there is a need to search for new peptides and peptidomimetics disrupting formation of the PD1/PD-L1 protein complex. Therefore, in the presented studies, we designed several peptides, specifically fragments of the PD-1 receptor, and assessed their binding to PD-L1 and their inhibitory properties towards PD-1/PD-L1 complex formation.

2. Results and discusion

2.1. MM/GBSA analysis performed for the PD-1/PD-L1 complex

To better understand the interactions between PD-1 and PD-L1 protein, all-atom molecular dynamics (MD) simulations of the PD-1/PD-L1 complex (PDB code: 4ZQK) were performed. The contribution of individual amino acid residues from PD-L1 to the binding affinity with PD-1 was estimated using the molecular mechanics generalized Born surface area (MM/GBSA) method. Initially, the pairwise per-residue energy decomposition (Fig. S1A) and the fraction of contacts (Fig. S1B) formed between PD-1 and PD-L1 in the complex were analysed. Furthermore, the per-residue energy decomposition was examined to investigate the total contribution of each amino acid of the PD-L1 (Fig. S2A) and PD-1 (Fig. S2B) proteins in formation of the PD-1/PD-L1 complex. Finally, by comparing the pairwise per-residue and the per-residue energy decomposition methods, the key residues in PD-L1 and PD-1 proteins were identified and are marked in bold in Table 1. Based on the analysis, fragments I54-Y56 and R113-R125 of the PD-L1 protein, and fragments N66-R86 and I126-E136 of PD-1 protein, are strongly involved in the interaction of both proteins. The structural representation of the most important amino acid residues involved in the PD-1/PD-L1 interaction, obtained from the MM/GBSA energy decomposition analysis, are shown in Fig. 1. It is worth noting that strong interactions between PD-1 and PD-L1 (black, blue, purple, and red areas) are distributed on their contact surface (PD-L1: R113, R125, K124, F19, D122; and PD-1: E136, E84, D77, Q75) and the residues that have the biggest contribution to the binding are located adjacent to each other.

According to the data published by Huang et al. [39] using interaction entropy MM/GBSA method-based computational alanine scanning there are eight hot spots in the PD-1 receptor, including amino acids N66, Y68, Q75, K78, E84, I126, L128, and I134, and one warm spot, namely K131, which interact with PD-L1. The energy component analysis of the computational alanine scanning shows the PD-1/PD-L1 interaction is dominated by van der Waals interactions between these amino acids but hydrogen bonds formed by E84, K78, and N66 are also important for binding of the proteins [39]. Our calculations further confirm Huang's results and in addition indicate, that the E136 in PD-1

Table 1
Key residues obtained from energy decomposition analysis determined using MM/GBSA. Residues marked in bold showed strong interaction in both per-residue and pairwise per-residue energy decomposition methods.

Type of the energy decomposition	Amino acid residues of PD-L1 involved in significant PD-L1/PD-1 interactions	Amino acid residues of PD-1 involved in significant PD-L1/PD-1 interactions
Per-residue	**F19,** Y56, **R113**, M115, **A121, Y123**, **R125**	N66, **Y68, Q75**, I126, L128, A132, I134, **E136**
Pairwise per-residue	A18, **F19**, D26, **R113, A121**, D122, **Y123,** K124, **R125**	**Y68**, **Q75**, D77, L79, E84, R86, **E136**

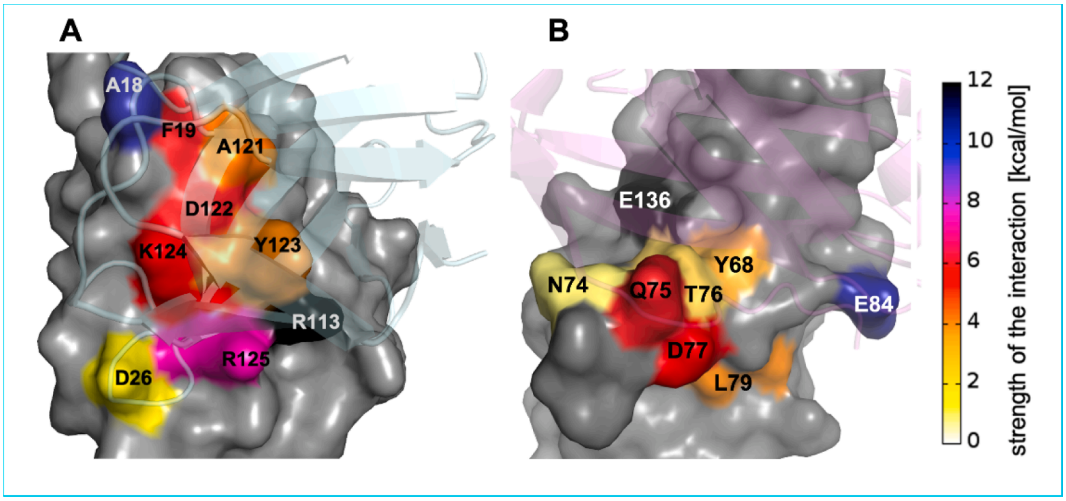

Fig. 1. Representations of the most important PD-L1 (A) and PD-1 (B) amino acid residues involved in PD-1/PD-L1 complex formation, based on the pairwise per-residue energy decomposition method. In Fig. 1A, the PD-L1 structure is represented by the surface area, and the PD-1 structure is shown in cartoon representation (semi-transparent, cyan). In Fig. 1B, the PD-1 structure is represented by the surface area, and the PD-L1 structure is shown in ribbon diagram (semi-transparent, violet). Surface areas of key residues are coloured according to the energy scale (shown on the side). (For interpretation of the references to colour in this figure legend, the reader is referred to the web version of this article.)

forms a very strong salt bridge with R113 (−11.303 kcal/mol) and with R125 (−7.319 kcal/mol), which suggests an important role of this residue in stabilizing the protein complex (Table S1). Huang et al. not only confirm these interactions but also point out that the substitution of E136 by alanine is favourable for the PD-1/PD-L1 interaction due to the benefits of van der Waals interactions and an entropy contribution. Our data further confirms the formation of hydrogen bonds and salt bridges between K78 and F19, D122 and A121. The importance of the K131 residue for PD-1/PD-L1 complex formation was not confirmed in our calculations.

Other studies, focusing on mapping the hot spots in the PD-1/PD-L1 complex, were performed by Ding and Liu [40]. They also confirmed that hot spots in PD-1 protein are Y68, Q75, I126, L128, I134, and E136 [40], which is fully consistent with our results. Moreover, they showed that the energetically dominant and hydrophobic residues of both proteins are packed together and form a hydrophobic core, whereas the energetically less important hydrophilic residues are located around it. Therefore, according to the authors, the hot regions of PD-1/PD-L1 are protected by a set of polar and energetically less important side chains which exclude solvent and protect the crucial interactions in the core [40].

In contradiction to our studies and those of others, the data obtained by Du et al. [41] using a molecular mechanics Poisson–Boltzmann surface area (MM/PBSA) methods indicate that other amino acids are hotspots. Their studies suggest that positively charged amino acids, such as K131, K135 and R104 in PD-1, are the key contributors to the binding energy. They also reported that Q75, T76, K78, D85 and E136 from PD-1 interact with PD-L1. It should be noted that, in the PD-1/PD-L1 crystal structure, the interactions found by Du et al. of amino acids K131, K135, R104 and D85 from PD-1 with PD-L1 protein have not been observed. The authors suggested that the data obtained from X-ray models are not sufficient to study protein/protein interactions and the contacts between amino acids observed in the crystal structure might not be the same as contacts created in solution under physiological conditions [41]. We also did not observe any relevance of these amino acids in MM/GBSA analysis [41].

2.2. Design and synthesis of peptides targeting PD-L1 protein

The crystal structure of PD-1/PD-L1 complex, and MM/GBSA calculations performed by us, enabled design of peptides which are potential inhibitors of the binding of these proteins. As reported previously, PD-1 protein has a β-sandwich structure and contains front and back β-sheets comprising CC′FG and AA′BDE strands, respectively. The PD-L1 binds to the front of the β-sheet containing CC′FG strands and the FG loop of the PD-1.

Taking this into consideration, we designed two groups of peptides which are potential inhibitors of PD-1/PD-L1 protein binding (Table 2). The first group contains amino acids from CC' β-sheets (peptides **1**–**4**, Table 2) and the second group was based on FG β-sheets and the FG loop (peptides **5**–**13**, Table 2) of PD-1 protein. For selected peptides, intramolecular disulfide bonds were introduced by replacing selected amino acids with cysteine residues. Disulfide bonds, created between the cysteines which are located opposite of each other should enable formation of a β-hairpin structure which mimics the structure of PD-1 protein. As reported previously the β-hairpin structure might be crucial for the interactions of peptides with β-sheet-rich protein surfaces, such as PD-L1 [42–44].

MM/GBSA analysis show that the crucial amino acids in the first group of peptides are Y68 and Q75 (Fig. S2). This information resulted in the design of two linear peptides, namely PD1(68–78) **(1)** and PD1 (62–80) **(2)**, which contain these residues. The first of these peptides possesses additionally, a D77 residue, and the second has N66, D77 and L79 amino acids, which are also important for the interaction of PD-1 with PD-L1. We also studied two peptides with disulfide bonds, namely PD-1(62–80)$^{W67C\text{-}L79C}$ **(3)** and PD-1(62–80)$^{R69C\text{-}D77C}$ **(4)**.

The second group of potential inhibitors was designed based on the *C*-terminal fragment of PD-1. We synthesized the linear peptide PD-1 (119–142) **(5)** and its analogues with intramolecular disulfide bonds, namely PD-1(119–142)$^{T120C\text{-}E141C}$ **(6)**, PD-1(119–142)$^{C123\text{-}S137C}$ **(7)** and PD-1(119–142)$^{A125C\text{-}K135C}$ **(8)**. The crucial residues in this fragment are I126, L128, A132, I134, E136 and they are all present in the designed peptides. The peptides **(7)** and **(8)** were poorly soluble in aqueous solution, (as found in later research) and for that reason we decided to study some shorter analogues of these, namely the peptides PD-1 (122–138) **(9)**, PD-1(122–138)$^{C123\text{-}S137C}$ **(10)**, PD-1(122–138)$^{A125C\text{-}K135C}$ **(11)** and PD-1(124–136)$^{A125C\text{-}K135C}$ **(12)**. Finally, we also tested the peptide PD-1(132–136) **(13)**, which contains only three amino acids important for binding of the proteins.

All the designed peptides were synthesized and purified, and selected peptides underwent an oxidation process to form disulfide bonds. The methionine in position 70 in the first group of peptides was replaced by

Table 2
The amino acid sequences of the designed peptides (Nle – norleucine, Abu – 2-aminobutyric acid).

No		Peptide	Amino acid sequence
1.	Group I	PD-1(68-78)	Ac-YRNleSPSNQTDK-NH_2
2.		PD-1(62-80)	Ac-SFVLNWYRNleSPSNQTDKLA-NH_2
3.		PD-1(62-80)$^{W67C-L79C}$	Ac-SFVLNCYRNleSPSNQTDKCA-NH_2
4.		PD-1(62-80)$^{R69C-D77C}$	Ac-SFVLNWYCNleSPSNQTCKLA-NH_2
5.	Group II	PD-1(119-142)	Ac-GTYLAbuGAISLAPKAQIKESLRAEL-NH_2
6.		PD-1(119-142)$^{T120C-E141C}$	Ac-GCYLAbuGAISLAPKAQIKESLRACL-NH_2
7.		PD-1(119-142)$^{C123-S137C}$	Ac-GTYLCGAISLAPKAQIKECLRAEL-NH_2
8.		PD-1(119-142)$^{A125C-K135C}$	Ac-GTYLAbuGCISLAPKAQICESLRAEL-NH_2
9.		PD-1(122-138)	Ac-LAbuGAISLAPKAQIKESLN-NH_2
10.		PD-1(122-138)$^{C123-S137C}$	Ac-LCGAISLAPKAQIKECL-NH_2
11.		PD-1(122-138)$^{A125C-K135C}$	Ac-LAbuGCISLAPKAQICESL-NH_2
12.		PD-1(124-136)$^{A125C-K135C}$	Ac-GCISLAPKAQICE-NH_2
13.		PD-1(132-136)	Ac-AQIKE- NH_2

its isostere - norleucine (Nle), as it is easily oxidated to methionine sulfoxide. The cysteine in position 123 in the second group of peptides was substituted by its isostere - 2-aminobutyric acid (Abu). In the PD-1 protein C123 forms a native disulfide bond with C54.

2.3. Studies of the interactions of PD-1-derived peptides with PD-L1 protein using SPR

In the next step, we studied the interaction of the designed peptides with PD-L1 protein using surface plasmon resonance (SPR). These analyses enabled us to assess the strength of protein/peptide binding, as determined by a K_D value. Binding analysis of the whole PD-1 protein (at concentrations from 30 nM to 4 μM) with PD-L1 immobilized to a sensor chip was performed (Fig. 2A). Subsequently, the kinetic constants were calculated (Fig. 2B). PD-1 protein interacts with PD-L1 protein, under the applied experimental conditions, with a K_D of 1.56 ± 0.96 μM. This value is comparable with the K_D of 1.15 ± 0.11 μM published previously by Li et al. [28], and somewhat lower to the data obtained by Cheng et al. [25], who reported that the K_D for PD-1/PD-L1 is 8.2 ± 0.1 μM. Despite these differences in K_D values, all the published data demonstrate that the proteins interact in the micromolar range.

In the next step, binding analysis of PD-L1 protein with a number of PD-1-derived peptides was performed. The obtained sensorgrams are presented in Fig. 3, and the K_D values, calculated for each PD-L1/peptide complex, are shown in Table 3. To compare the binding of peptides with PD-L1 protein as a referring point the K_D obtained by us for proteins

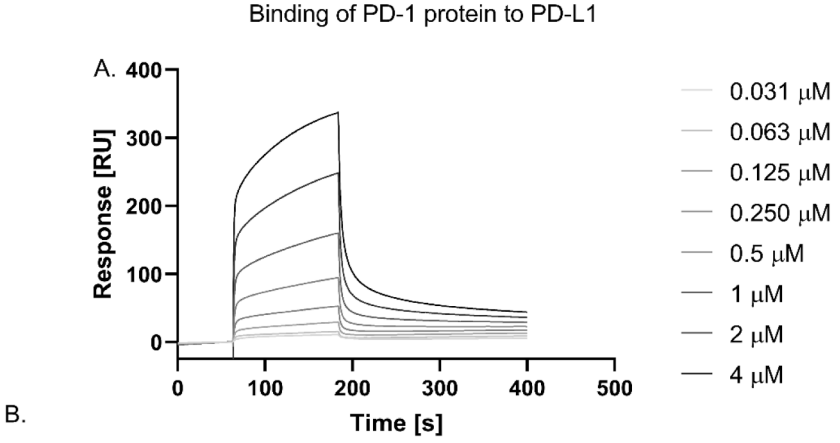

B.

Protein	ka ($M^{-1}s^{-1}$)	SD	kd (s^{-1})	SD	K_D (M)	SD
PD-1	3.30×10^{4}	4.93×10^{4}	2.13×10^{-2}	2.06×10^{-2}	1.56×10^{-6}	9.60×10^{-7}

Fig. 2. SPR analysis of PD-1 protein binding to PD-L1. (A) Sensorgrams showing the increase in the detected signal, indicating PD-1 binding to PD-L1 immobilized on the surface of a sensor chip. (B) Kinetic constants calculated from the obtained SPR data with Biacore T200 Evaluation Software.

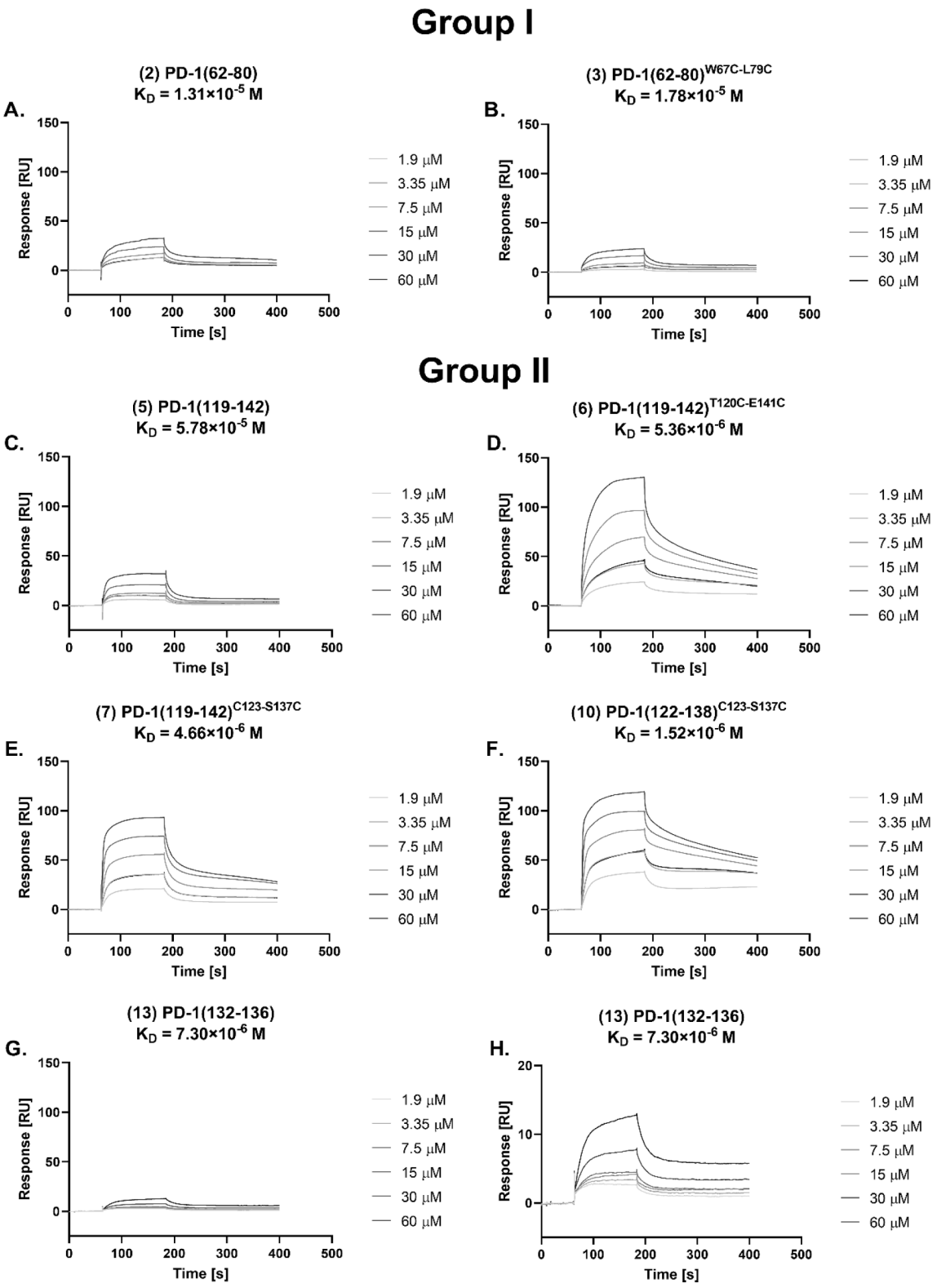

Fig. 3. Binding of PD-1 peptides to PD-L1 protein, analyzed by SPR. The binding of peptide PD-1(132–136) is shown on different scales. The fitting of theoretical curves to obtained results are presented in Fig. S5.

complex was used. Additionally, as a positive control we used the BMS pep-57 (Fig. S3). The compound interacts with PD-L1 protein, under the applied experimental conditions, with a K_D of 62.8 nM. This K_D value is lower comparing with the K_D of 19.9 nM published previously by Ganesan et al. [45]. However, the authors performed the analysis using Fc-PD-L1 (here the His-PD-L1 was used), which could have influence on the binding kinetic.

Peptides from the first group bind to PD-L1 protein with a lower affinity than the PD-1 receptor, or do not interact at all with it. The affinity of the peptide **(2)** for PD-L1 is about 8-times weaker (K_D 13.1 ± 12.7 μM) than PD-1, while its shorter analogue - peptide **(1)** - does not bind to the ligand (Fig. S4). When considering those peptides with

Table 3
Kinetic constants calculated from SPR data for PD-1 protein fragments (peptides) binding to PD-L1 protein immobilized on a CM5 sensor chip surface. Constants were calculated with Biacore T200 Evaluation Software using data from at least three separate titration analyses. The 1:1 binding model was applied. SD – standard deviation, ND - not determined (there was no binding or binding was too weak to determine reliable constants).

	No	Peptides	k_a ($M^{-1}s^{-1}$)	SD	k_d (s^{-1})	SD	K_D (M)	SD
Group I	**1.**	PD-1(68–78)	ND	ND	ND	ND	ND	ND
	2.	PD-1(62–80)	2.18×10^2	2.77×10^2	1.76×10^{-3}	1.08×10^{-3}	1.31×10^{-5}	1.27×10^{-5}
	3.	PD-1(62–80)$^{W67C\text{-}L79C}$	4.94×10^2	4.20×10^2	9.19×10^{-3}	1.18×10^{-2}	1.78×10^{-5}	1.36×10^{-5}
	4.	PD-1(62–80)$^{R69C\text{-}D77C}$	ND	ND	ND	ND	ND	ND
Group II	**5.**	PD-1(119–142)	1.45×10^2	1.50×10^2	4.27×10^{-3}	1.07×10^{-3}	5.78×10^{-5}	4.11×10^{-5}
	6.	PD-1(119–142)$^{T120C\text{-}E141C}$	9.97×10^2	7.00×10^2	3.17×10^{-3}	5.58×10^{-4}	5.36×10^{-6}	4.02×10^{-6}
	7.	PD-1(119–142)$^{C123\text{-}S137C}$	6.76×10^2	2.20×10^2	2.86×10^{-3}	2.48×10^{-4}	4.66×10^{-6}	1.97×10^{-6}
	8.	PD-1(119–142)$^{A125C\text{-}K135C}$	Not soluble in solution using in SPR measurement					
	9.	PD-1(122–138)	ND	ND	ND	ND	ND	ND
	10.	PD-1(122–138)$^{C123\text{-}S137C}$	1.21×10^3	1.08×10^2	1.80×10^{-3}	9.91×10^{-4}	1.52×10^{-6}	8.76×10^{-7}
	11.	PD-1(122–138)$^{A125C\text{-}K135C}$	ND	ND	ND	ND	ND	ND
	12.	PD-1(124–136)$^{A125C\text{-}K135C}$	ND	ND	ND	ND	ND	ND
	13.	PD-1(132–136)	2.23×10^2	1.02×10^2	1.25×10^{-3}	4.26×10^{-4}	7.30×10^{-6}	5.47×10^{-6}

disulfide bonds, the peptide **(4)** does not interact with PD-L1 (Fig. S4) and the affinity of peptide **(3)** is comparable to peptide **(2)** (17.8 ± 13.6 μM). The sensorgrams obtained for those peptides which interact with PD-L1 protein are shown in Fig. 3, and all determined kinetics constants are presented in Table 3.

Among the peptides from the second group, peptide **(10)** shows the highest affinity to PD-L1 protein, which is indicated by the highest k_a and the lowest K_D values. Moreover, the resonance units (RU) obtained after injection of this peptide onto a surface with immobilized PD-L1 protein were the highest (Fig. 3). It interacts with PD-L1 protein with a K_D of 1.52 ± 0.88 μM, which is comparable to the strength of PD-1/PD-L1 binding determined by us and by Zhu et al. [28]. Similar affinity to PD-L1 was observed for the peptides **(7)** and **(6)**. They bound to PD-L1 with lower affinity than PD-1 receptor and peptide **(10),** with K_D values of 4.66 ± 1.97 μM and 5.36 ± 4.02 μM, respectively. Peptide **(5)** also interacts with PD-L1, but its affinity to this ligand was lower than the aforementioned compounds and the determined K_D value was 57.8 ± 41.1 μM. Peptides **(9)**, **(11)** and **(12)** show no binding to PD-L1 protein (Fig. S4) and for those peptides the kinetic constants were not determined (Table 3). The analogue **(8)** was not soluble in standard buffers used in SPR analyses, and therefore its binding to PD-L1 was not measured.

Binding of peptide **(13)** was not easily discernable, as the response obtained after injection of the highest concentration of peptide was 13 RU (Fig. 3F and G). However, taking into consideration that the molecular mass of this peptide is less than one-third of the other studied compounds, and that the response depends on the molecular mass of an analyte interacting with a ligand, it can be concluded that **(13)** interacts with PD-L1 with a K_D of 7.30 ± 5.47 μM.

In many reports the K_D value determined by SPR is the first step in evaluating the potential inhibitory properties of compounds. Herein we compare the strength of peptides affinity obtained by us with the literature reports. Chang H-N et al. [46] studied a series of D-peptides obtained using mirror-image phage display technology. Two of them, namely PPA-1 and PPA-2, bind to PD-L1 protein with K_D values of 0.51 μM and 1.13 μM respectively, which are comparable to the K_D obtained for peptide **(10)** (1.52 μM). PPA-1 possesses the ability to inhibit PD-1/PD-L1 interaction in in vitro cell assays, while for PPA-2 these properties were not observed. In addition, experiments in tumour-bearing mice models showed that PPA-1 could inhibit CT26-tumour growth and prolong animal survival [46]. Li et al. [28] described the peptide Ar5Y_4, which interacts with PD-1 receptor with a K_D value of 1.38 μM. This peptide inhibits PD-1/PD-L1 complex formation in SPR competitive binding assays and restores the function of suppressed Jurkat E6.1 cells, which makes it a promising candidate for cancer immunotherapy [28]. Kotraiah et al. [47] reported a series of peptide-based PD-1 immunomodulators obtained by screening random peptide phage libraries. Four peptides, namely WQ-20, QP-20, HD-20 and SQ-20, interact with PD-1 receptor with K_D values from 3.40 μM to 305 μM. These peptides also have the ability to block the binding of PD-L1 to PD-1 in cellular studies using PD-1-expressing Jurkat E6.1 effector cells and PD-L1-expressing Chinese hamster ovary (CHO) cells. Moreover, the authors studied the bioactivity of the peptides in vivo, using the B16-F10 syngeneic mouse melanoma model, and they showed that a combination of the four peptides led to fewer surface tumour metastases compared to groups receiving anti-PD1 mAb [47].

2.4. The stability of the selected PD-1 derived peptides and their effects on the viability of CHO-K1 and Jurkat E6.1 cell lines

The cellular studies described in the next part of this work were performed using modified CHO-K1 and Jurkat E6.1 cell lines cultured in RPMI (Roswell Park Memorial Institute) 1640 medium. At first, we checked the stability of the peptides in the RPMI 1640 medium with 10% heat-inactivated fetal bovine serum (FBS) and their effect on the viability of the aforementioned cell lines used in a PD-1/PD-L1 blockade bioassay. For these studies we chose only those peptides showing affinity to PD-L1 protein - peptides **(2)** and **(3)** from the first group, and peptides **(5)**, **(6)**, **(7)**, **(10)** and **(13)** form the second group. The stability of the peptides was investigated at time 0 and after 24 h incubation in RPMI 1640 medium, using reversed phase-high performance liquid chromatography (RP-HPLC) methods. To determine the stability of the peptide the peak area of the peptide dissolved in H_2O (control) was compared with the peak area of the peptide dissolved in medium at the appropriate time. The obtained data are presented in Fig. 4.

Two peptides, namely **(3)** and **(13)**, show the highest stability in RPMI medium at time 0 (96% and 100%, respectively) and after 24 h incubation (86% and 96%, respectively), in comparison to the control. In contrast, the biggest changes in concentration were observed for the linear peptides **(2)** and **(5)** (Fig. 4 and S6). For peptide **(2)** the concentration decreased by about 42% at time 0 and by about 62% after 24 h of incubation. For peptide **(5)** the reduction of concentration at time 0 was mildly decreased (about 10%), but after 24 h of incubation only 43% of the initial amount of peptide was observed in the sample. The peptides **(6)**, **(7)** and **(10)**, with disulphide bonds, show a decrease in concentration of about 19–38% at time 0 and 37–50% after 24 h of incubation. As mentioned previously in numerous publications, peptides can be subjected to many chemical and biological processes in solution [48–50]. It should be noted that, in our studies, additional signals in HPLC chromatograms, indicating the degradation process, were not noticed, but a reduction in the signal was observed. This might suggest that the peptides or peptide degradation products interact with some components of the medium. Binding of the peptides to serum albumin proteins was previously observed by us for other peptides [51].

Subsequently, we investigated the effects of peptides on the viability of CHO-K1 and Jurkat E6.1 cells using the CellTiter-Glo® Luminescent

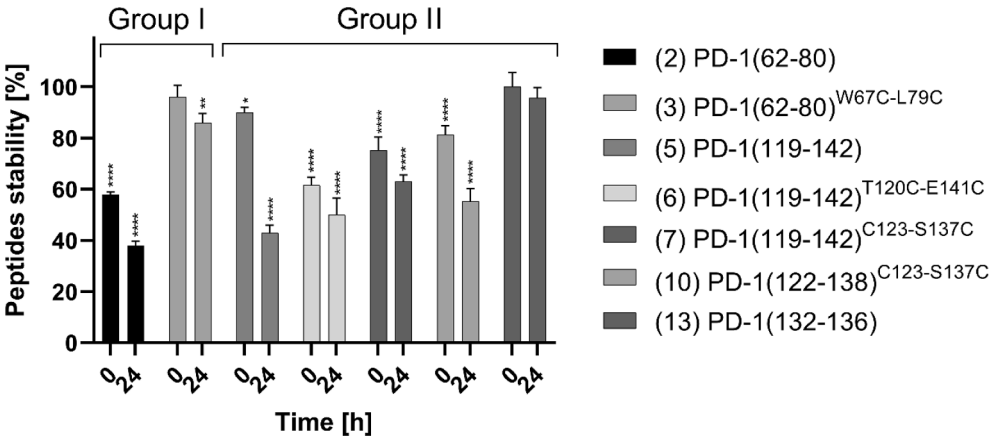

Fig. 4. Stability of the peptides in RPMI 1640 medium at time 0 and 24 h, determined using RP-HPLC methods. In the graphs the percentage of peptide remaining in the sample at time 0 and 24 h after incubation is shown. The stability was determined in relation to control (appropriate peptide, diluted in H_2O, at time 0, at the same concentration). Results are shown for three experiments performed independently. Data are depicted as mean with SD (Mean +/-SD). Statistical analysis was performed using one-way analysis of variance (ANOVA) followed by Dunnet's post-hoc test. ****: $p < 0.0001$, ***: $p < 0.001$, **: $p < 0.01$, *: $p < 0.05$.

Cell Viability Assay from Promega Corporation. This test allowed us to determine the number of viable cells in the presence and absence of peptides, based on quantitation of adenosine triphosphate (ATP), which is an indicator of metabolically active cells and is proportional to the number of cells present in the culture [52]. Six different concentrations of the peptides were tested (150, 50, 16.7, 5.6, 1.9 and 0.62 μM). Peptides from the first group, namely **(2)** and **(3)**, did not have an effect on the viability of the analysed cells at concentrations from 50 μM to 0.62 μM (Fig. 5A, B and 6A, B). A small reduction in cell viability was observed only for the highest concentration of peptide **(2),** where it was 20% and 17% for CHO-K1 and Jurkat E6.1 cells, respectively. The peptides **(5)**, **(7)** and **(13)**, from the second group, at a concentration of 150 μM, significantly reduced CHO-K1 cell viability by about53 % (Fig. 5C), 24% (Fig. 5E) and 67% (Fig. 5G), respectively. Moreover, the peptides **(6)** and **(10)** at this concentration had a cytotoxic effect on CHO-K1 cells (Fig. 5D and 5F). Slightly negative effects on cell viability were observed for the peptides **(5)**, **(6)**, **(7)** and **(10)** at the 50 μM concentration. For the Jurkat E6.1 cells the decrease in viability in the presence of these peptides was not as significant as for CHO-K1 and the most pronounced effect was observed for the peptides **(5)**, **(7)** and **(10)** at a concentration of 150 μM (Fig. 6C, 6E and 6F). Lower concentrations of the peptides did not have such a significant impact on viability of Jurkat E6.1 cells (Fig. 6). In comparison with data published for the macrocyclic peptides BMS pep-57, p101 and p104 (patented by Bristol-

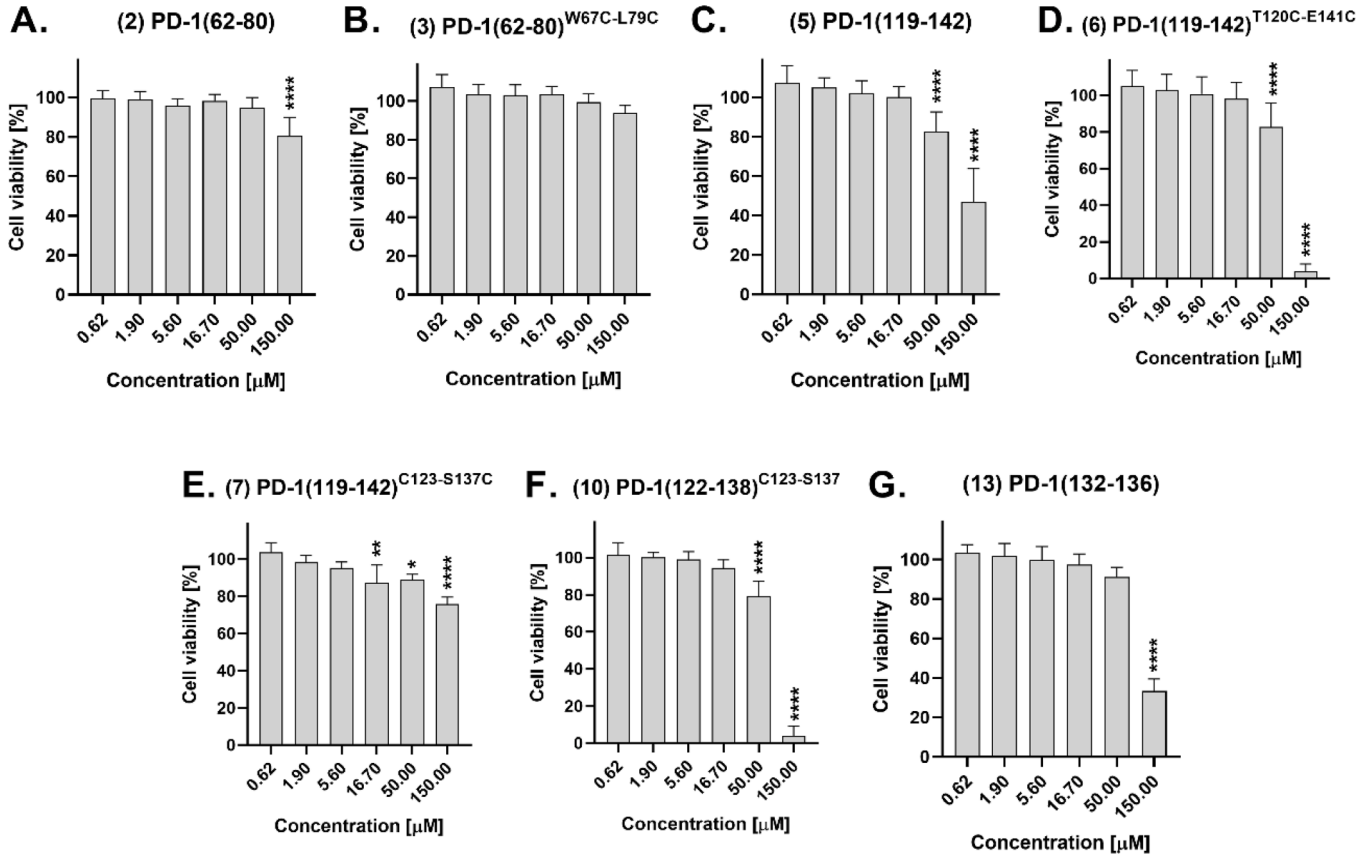

Fig. 5. The effect of peptide fragments of PD-1 protein on CHO-K1 cell viability, determined using the CellTiter-Glo® Luminescent Cell Viability Assay. Results are shown for three experiments performed independently, in triplicate. Data are depicted as mean with SD (Mean +/-SD). Statistical analysis was performed using one-way analysis of variance (ANOVA) followed by Dunnet's post-hoc test. ****: $p < 0.0001$, ***: $p < 0.001$, **: $p < 0.01$, *: $p < 0.05$.

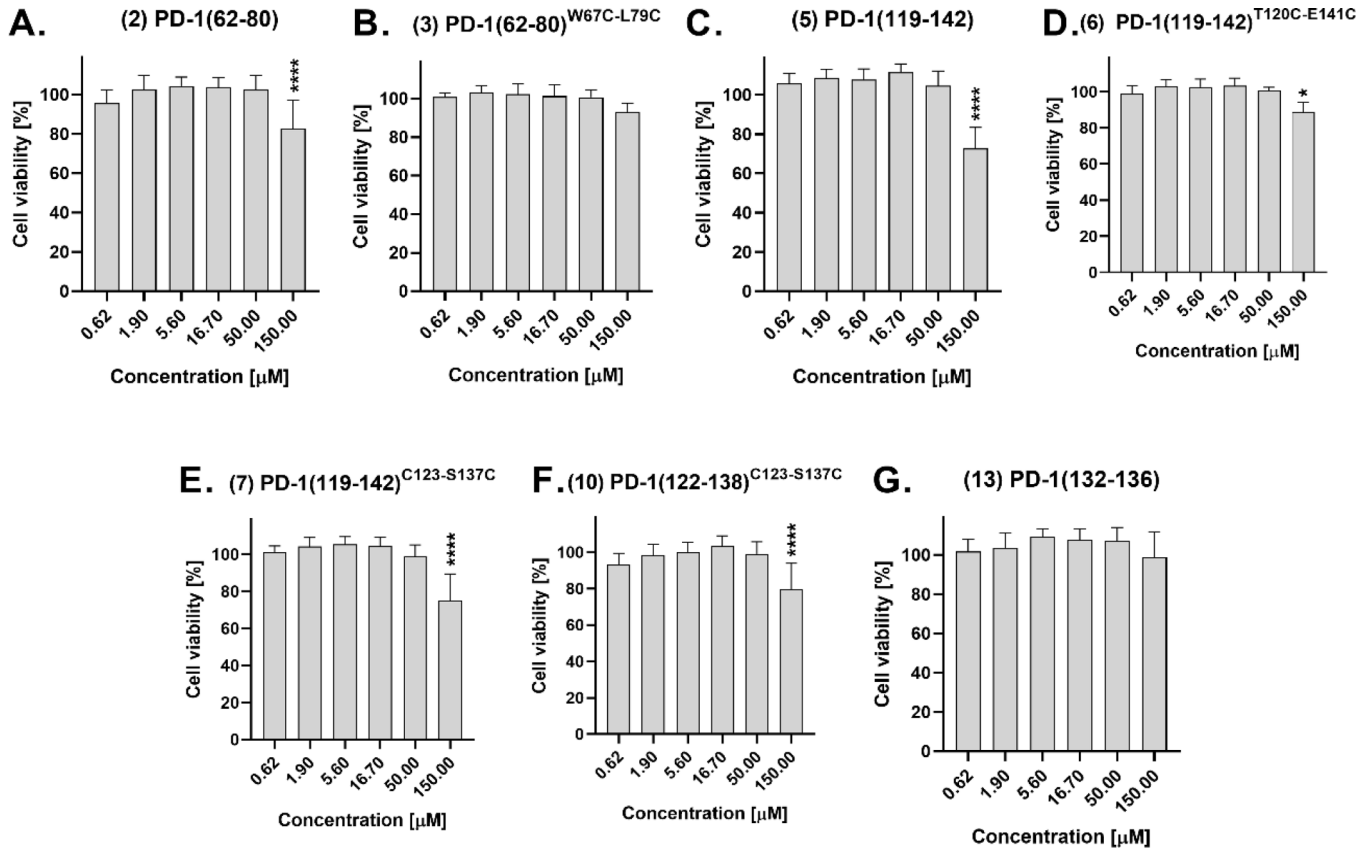

Fig. 6. The effect of peptide fragments of PD-1 protein on Jurkat E6.1 cell viability determined using the CellTiter-Glo® Luminescent Cell Viability Assay. Results are shown for three experiments performed independently, in triplicate. Data are depicted as mean with SD (Mean +/-SD). Statistical analysis was performed using one-way analysis of variance (ANOVA) followed by Dunnet's post-hoc test. ****: $p < 0.0001$, ***: $p < 0.001$, **: $p < 0.01$, *: $p < 0.05$.

Myers Squibb), and tested in independent research by Ganesan et al. [45], Magiera-Mularz et al. [53] and Zyla et al. [33], respectively, our peptides exhibited weak cytotoxic effect on CHO-K1 and Jurkat E6.1 cells. However, the highest tested concentration for BMS pep-57 was 10 μM, considerably lower than the concentration applied by us. At this concentration there was no negative effect on either CHO-K1 or Jurkat E6.1 cells, when exposed to all of the peptides. To sum up, our results demonstrate that some peptides decrease cell line viability at a concentrations of 150 μM. From that we decided that 50 μM would be the highest concentration of compound used in inhibitory studies using the aforementioned cell lines.

2.5. Bioluminescent cell-based PD-1/PD-L1 immune checkpoint blockade assay

The inhibitory properties of the selected peptides (**2**, **3**, **5**, **6**, **7**, **10** and **13**) were studied using a bioluminescent PD-1/PD-L1 blockade bioassay (Promega). This test is based on two genetically engineered cell lines, namely effector Jurkat E6.1 cells expressing human PD-1 and a luciferase reporter driven by an NFAT response element (NFAT-RE), and aAPC/CHO-K1 cell lines expressing PD-L1 and a protein designed to activate TCR/CD3 complex in an antigen-independent manner. Co-culture of these two cell lines leads to binding of PD-L1 to PD-1, which causes inhibition of TCR signalling and results in inhibition of NFAT-RE-mediated luminescence. Blocking of the PD-1/PD-L1 interaction restrains the inhibitory signal which results in TCR activation and NFAT-RE-mediated luminescence. For the blockade assay, concentrations of peptides from 50 μM down to 0.62 μM were chosen. As described earlier, higher concentrations of the peptides were cytotoxic. In the cellular assay, target cells (aAPC/CHO-K1) expressing PD-L1 protein were cultured overnight. The PD-1 derived peptides, which interact with PD-L1 protein, were applied to the target cells at five different concentrations and preincubated for 1.5 h. Jurkat E6.1 cells expressing PD-1 protein were then added and after 6 h of incubation the luminescence signals were measured. The obtained results are presented as the fold induction dependent on the concentration of the peptide. Anti-PD-1 antibody was used at three concentrations 1.25 μg/mL, 0.125 μg/mL and 0.0125 μg/mL, as a control (Fig. 7H). The data show that the peptides **(7)** and **(10)** inhibit the PD-1/PD-L1 interaction in a dose-dependent manner, resulting in enhanced T cell activation (Fig. 7). It should be noted that both of these peptides have disulphide bonds in the same positions in their amino acid sequences and differ in the presence or absence of *N*- and *C*-terminal residues. Dose-dependent inhibitory properties were also observed for the linear peptide **(5)** at concentrations from 16.7 μM to 0.62 μM but not at the 50 μM (Fig. 7). This might be due to the small cytotoxic effect of that peptide on the CHO-K1 cell line, which is about 17% at a concentration of 50 μM (Fig. 5).

The peptides **(10)** and **(7)** have the best inhibitory properties towards PD-1/PD-L1 complex formation and also show the strongest binding to PD-L1 protein (K_D 1.52 μM and K_D 4.66 μM, respectively). A lack of ability to disrupt interaction of these proteins in the blockade assay was observed for peptide **(6)**, whose affinity to PD-L1 protein was also in the micromolar range of magnitude (K_D 5.36 μM). Peptides **(7)** and **(10)** had limited effect in the blocking assay, and their fold induction at the highest concentration is about 1.2. For comparison, the peptides published by Kotraiah et al., which possess K_D values from 3.40 μM to 305 μM, disrupt the PD-1/PD-L1 binding better than peptides **(10)** and **(7)**, although their interaction with PD-L1 protein as determined by SPR is weaker [47]. For all peptides tested by Kotraiah et al. the fold induction was more than 1.5 at the same concentration of peptides. In addition, for the macrocyclic peptides BMS pep-57, BMS pep-71 and BMS pep-99 by Bristol-Myers Squibb and studied by Magiera-Mularz

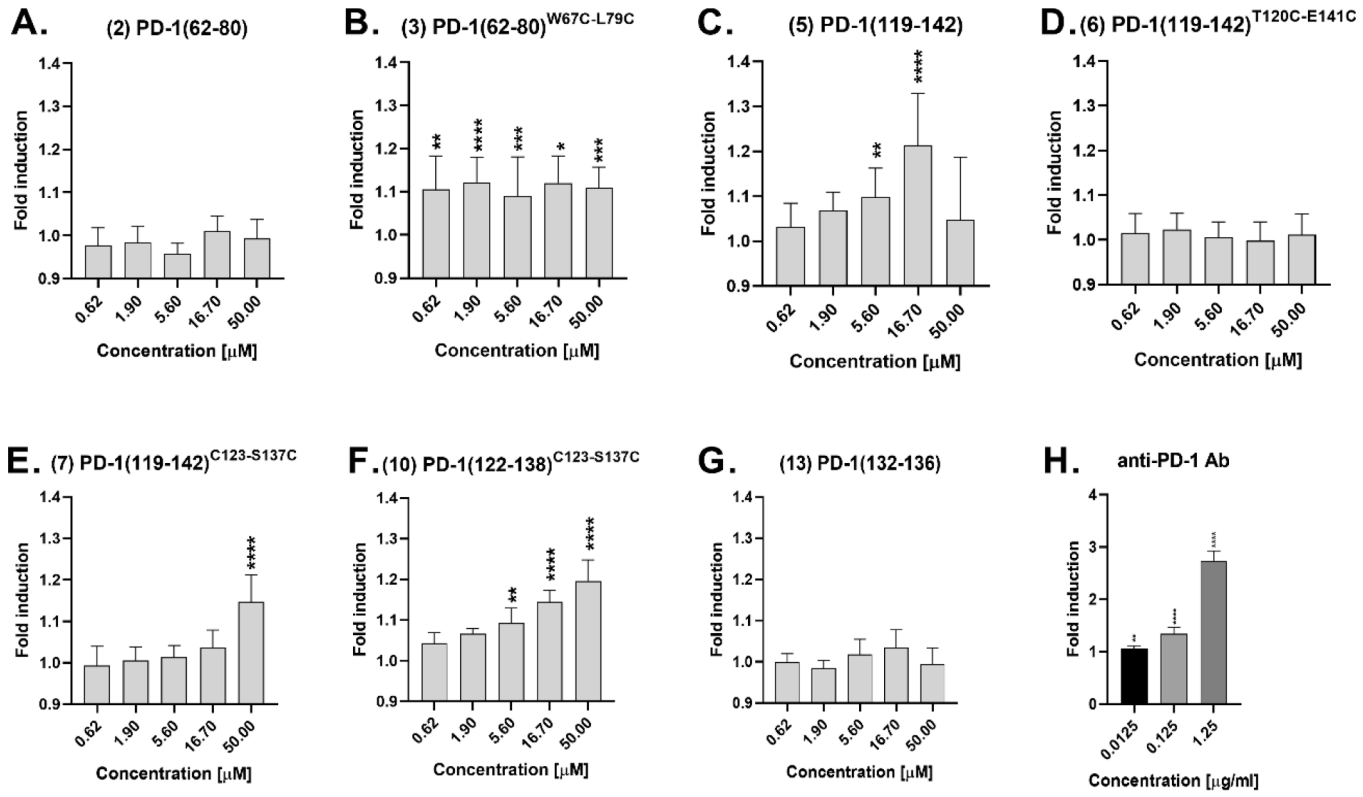

Fig. 7. The inhibitory properties of the PD-1-derived peptides, determined from PD-1/PD-L1 blockade bioassay. The data are shown as the fold induction and were calculated by dividing the RLU of the cells treated with peptides at the appropriate concentration by the RLU of the untreated cells (RLU peptide/RLU control), where the RLU is relative luminescence units. Results are shown for three experiments performed independently, in duplicate. Data are depicted as mean with SD (Mean +/-SD). Statistical analysis was performed using one-way analysis of variance (ANOVA) followed by Dunnet's post-hoc test. ****: $p < 0.0001$***: $p < 0.001$, **: $p < 0.01$, *: $p < 0.05$.

et al., the maximal activity levels defined as RLU are between 2.62 and 3.25 [54]. All these data suggest that the peptides **(10)** and **(7)** could be good candidates to be anti-cancer drugs, but their structure requires further optimization. To this end, NMR techniques and molecular modeling studies were used to obtain the molecular details of the peptide/PD-L1 interactions.

2.6. Conformation studies of peptide PD-1(122–138)$^{C123\text{-}S137C}$ using NMR and molecular dynamics

NMR studies provide information regarding peptide conformation which can subsequently be used to dock a peptide to a target protein leading to identifying its binding spot. We used NMR to determine the 3D structure of peptide **(10)**. This peptide was chosen for further research due to the fact that it is a shorter analogue of peptide **(7)** with a disulfide bond in the same position, and both peptides have the best inhibitory properties among the compounds analyzed here. However, peptide **(10)** is characterized by better solubility in aqueous solutions, which is an important feature for a potential drug candidate.

Detailed analysis of the NMR data for peptide **(10)**, and the procedure for calculating the 3D NMR structure, can be found in the Supplementary materials. It is worth mentioning that the NMR data confirmed the presence of all peptide bonds in the *trans* geometry and that the thiol groups exist in the oxidized state. The obtained conformations were clustered into 10 conformational families, two of which together accounted for 72% of conformations and were considered in further analysis and a docking procedure (Fig. S7). Due to the presence of a disulfide bridge and intramolecular hydrogen bonds both conformational families form a β-hairpin-like structure.

The peptide conformations were docked to PD-L1 protein using a UNited RESidue (UNRES) force field and then multiplexed-replica exchange molecular dynamics (MREMD) were performed. In this way, we were able to identify the PD-L1/peptide binding interface. Three types of structures of peptide **(10)** were used in the docking procedure to generate restraints. The first was peptide **(10)** cut from the crystallographic structure of the PD-1/PD-L1 complex (PDB code: 4ZQK), in which the appropriate amino acids residues were replaced by cysteines, while the second and third were the NMR structures (both families) described above. The PDB based structure restraints served as a positive control system. The molecular docking of peptide **(10)** to PD-L1 was performed with weak restraints on the torsional and valence angles of the backbone and weak restraints on the side chain–side chain and peptide group–peptide group contacts based on the structure of PD-L1 and the peptide. It should be noted that no restraints were imposed on the protein–peptide interface. To validate the docking method, the same procedure was performed for peptide **(4)**, which does not bind to the PD-L1 protein according to our SPR data. The structure of peptide **(4)** was cut from the crystal structure of PD-1/PD-L1 and the cysteine residues were introduced in appropriate positions in the amino acid sequence. In the case of all-docked conformations of peptide **(10)** at least one cluster in each docked complex displayed high similarity with the PD-1/PD-L1 one (Table 4, Fig. 8). It can be seen that the complex, with the docked structure cut from the PD-1 protein, is the most similar to the native PD-1/PD-L1 complex (Fig. 8B, RMSD 0.93 Å). The complexes possessing the best root-mean-square deviation (RMSD) values were obtained for both families of peptide (10) received from NMR data (Table 4, Fig. 8). Peptide **(4)** has the highest RMSD values, which confirm our SPR results.

In addition, the association, dissociation and equilibrium dissociation constants for peptide **(10)** were determined using UNRES force field canonical molecular dynamics. The constants were fixed for the peptide conformations based on the crystal structure of PD-1 protein, family 1 from the NMR data and family 2 from the NMR data. The strongest

Table 4
Root-mean-square deviations between the clusters obtained from the MREMD simulations and the appropriate PD-1/PD-L1 crystal structure interface.

Cluster	Peptide **(10)** based on crystal structure	Peptide **(10)** based on family 1 from NMR	Peptide **(10)** based on family 2 from NMR	Peptide **(4)** based on crystal structure – control
best similarity	0.93 Å	2.62 Å	3.65 Å	4.15 Å
dominant	5.43 Å	4.12 Å	4.26 Å	8.74 Å

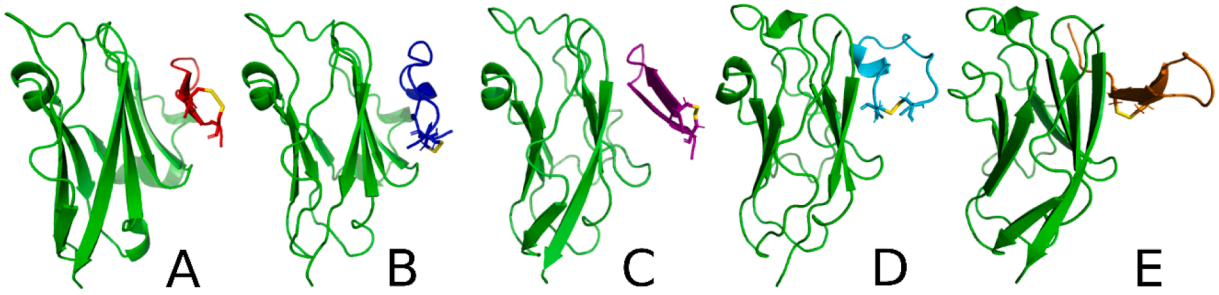

Fig. 8. The structure of PD-L1 protein and peptide. The structure of the peptide was obtained from: (A) trimmed PD-1 structure to match the peptide **(10)** sequence. Points B-E show the cluster representative structure after MREMD simulation with the lowest RMSD to crystal like structure for different restrains used: (B) fragment of the crystal structure of protein PD-1 with sequence of peptide **(10)**, (C) NMR family 1 restraints on peptide **(10)**, (D) NMR family 2 restraints on peptide **(10)**, (E) fragment of the crystal structure of protein PD-1 with sequence of peptide **(4)-** control.

binding to PD-L1 protein was observed for the peptide conformations from NMR family 1. The binding of the crystal-like structure to PD-L1 is stronger than that of NMR family 2 and significantly stronger than that of peptide **(4)** (Table S3). It should be noted that when peptide **(10)** binds with restraints from the NMR data the association rate constant is about 10 times lower in comparison to the restraint from the crystal structure, indicating that some conformational reorganization occurs in the process of binding. In the presented analyses, the peptide **(4)** was used as a control, and since it interacts with PD-L1 protein at least 10 times more weakly than the peptide (**10**) restraints based on the crystal structure (Table S3).

A reverse approach to the design of inhibitors of PD-1/PD-L1 complex formation was followed by Boohaker et al. [55]. Based on the structure of the protein complex, sequences of short peptides, which mimic PD-1 protein, were designed, and then the structures of these peptides were docked to the appropriate proteins: PD-1 or PD-L1. The authors initially determined the thermodynamic parameters for the peptide-protein complexes and then confirmed these theoretical data by experimental studies. They used different linear amino acid sequences, calculation methods and tools, and therefore we cannot directly compare our results. However, it is worth emphasizing that molecular modeling methods enabled them to obtain peptides with anti-tumour activity, which could constitute an alternative to antibody-based immunotherapies [55].

Liu et al. [56] also used the docking procedure to assess the protein/peptide binding site and explain the lack of inhibitory activity for some peptides. They used peptides interacting with PD-L1, identified using phage display. The strongest inhibitors bound to the PD-1/PD-L1 protein contact surface whereas the non-inhibitory peptides bound in sites other than the PD-1/PD-L1 protein contact surface or with a lower binding constant [56]. The body of research proves that molecular modeling methods constitute a reliable tool to predict the inhibitory properties of compounds.

Recent studies have shown that the pH of cancer microenvironment may affect the interaction of PD-L1 inhibitors [57], for that we checked the protonation state of PD-1, PD-L1 and peptide **(10)** in different pH using APBS server [58]. As was reported, in tumor microenvironment, extracellular pH decreases to acidic values below 7.0 [59–61]. Therefore we analyzed the protonation state in pH 6.0, 7.0 and 8.0. Our data indicate that considering the interaction of PD-L1 with our peptide inhibitors, only the H69 residue may potentially have influence on the peptide binding. The side chain of H69 is about 6.4 Å away from the nearest O atom from the peptide group. This indicates that pH 6.0 could enhance the binding strength between the peptide **(10)** and PD-L1 protein (Fig. S13). In presented analysis we considered the structure of peptide **(10)** from NMR data. The more broad discussion regarding protonation state depending on pH is presented in Supplementary materials.

3. Conclusion

Peptides as therapeutics have many advantages, including high selectivity for target molecules, low accumulation in tissues and well-known metabolic pathways comparing to small molecules. Another advantage of peptides is a synthesis protocol, which is standardized, optimized and relatively easy to modify, and has lower costs of production [35,62–64]. Peptides achieve good tumour penetration and they exhibit a short pharmacokinetic profile putatively leading to fewer unwanted immune-related adverse effects (irAEs) comparing to antibodies [65]. Taking into account their advantages, peptides could be an alternative to antibodies and small compounds in cancer immunotherapy.

In the presented studies we designed, synthesised and tested peptides which are fragments of the PD-1 receptor and interact with PD-L1. Disulphide bonds were introduced to most of the peptides to enable formation of a β-harpin structure, similar to the binding fragments of PD-1 protein. Three of these, namely peptides **(6)**, **(7)** and **(10)** interact with PD-L1 in the micromolar range, which is comparable to PD-1/PD-L1 binding. Studies of the viability of CHO-K1 and Jurakt E6.1. cell lines studies showed that the peptides **(5)**, **(6)**, **(10)** and **(13)** are cytotoxic for the studied cells at concentrations of 150 μM. The other concentrations of compounds do not have the significant impact on cell survival. We observed that the concentration of peptides decreased during incubation in the cell culture medium, which could suggest that they/or their degradation products interact with some medium components. Studies using a bioluminescent cell-based PD-1/PD-L1 immune checkpoint blockade assay revealed that the best inhibitory properties were possessed by peptides **(7)** and **(10)**. They disrupt the binding of the proteins in a dose-dependent manner, but their blocking capacities are rather weak in comparison to antibodies. Regardless of that, we decided to study the molecular details of the interactions of peptide **(10)** with

PD-L1. To do this, the 3D structure of peptide **(10)** was initially determined using NMR techniques and then the obtained conformations were docked to PD-L1 protein. All the data show that peptide **(10)** possesses a well-defined structure and interacts with PD-L1 in the same place as does PD-1 protein. In the future this knowledge should be useful in the design of new peptides/peptidomimetics with better inhibitory capacities.

4. Materials and methods

4.1. MD simulation protocol

All-atom molecular dynamics simulation of the PD-L1/PD-1 complex (PDB: 4ZQK) was performed using the AMBER16 software package [66]. A truncated octahedron TIP3P periodic box of 10 Å water layer from the box's border to the solute was used to solvate the complex. The complex structure was minimized in the AMBER ff14SB force field, initially with positional Cα constraints of 10 kcal/(mol × $Å^2$) (steepest descent for 1500 steps and conjugate gradient for 1000 steps), and then without restraints (steepest descent for 6000 steps and conjugate gradient for 3000 steps). After these minimizations the system was heated up from 0 to 300 K for 10 ps with positional restraints and then equilibrated with NPT MD simulations (constant number of particles, under a constant pressure of 105 Pa and with a constant temperature of 300 K) without constraints for 0.5 ns. An 8 Å cutoff for nonbonded interactions and the particle mesh Ewald method for long-range electrostatic interactions were applied. MD simulations were performed using an ff14SB force field [67,68] for 360 ns under NPT conditions in explicit water TIP3P (with a SHAKE algorithm to perform bond length constraints where covalent bonds involving hydrogen are constrained), using Langevin dynamics (with the collision frequency equal to 1 ps^{-1}) and a Berendsen barostat for both systems.

4.2. Binding free-energy calculations

The free energy calculations (binding free energy) were performed with MM-GBSA [69] using a model with surface area and Born radii default parameters as implemented in the igb = 2 model in AMBER16 [70]. The energy was decomposed according to the per-residue and pairwise per-residue schemes, taking into account local (between 1 and 4 atoms) electrostatic and local van der Waals energies. All frames from the MD simulations were analysed. Data analysis and its graphical representation were performed using PyMOL (The PyMOL Molecular Graphics System, Version 1.2r3pre, Schrödinger, LLC) and VMD [71].

4.3. Post-processing of the MD trajectory

Contact analysis of the MD trajectory was performed using the CPPTRAJ program [72], which was designed to process coordinate trajectories and data files generated using the AMBER package. Contacts between PD-L1 and PD-1 amino acid residues were traced as any heavy atom pair (i.e., any atoms except hydrogen atoms) closer than 4 Å from each other.

4.4. Peptide synthesis

Peptides syntheses were performed using a solid-phase peptide synthesis (SPPS) protocol on an automated microwave peptide synthesizer (LibertyBlue, CEM Corporation, Matthews, NC, USA). Peptides were synthesised on a TentaGel R RAM resin (0.21 mmol/g) using Fmoc/tBu chemistry and standard amino acid derivatives. The *N*-terminal amino group of the peptidyl-resin was acetylated using a solution of 1-acetylimidazole (1.10 g/1 g of resin at room temperature for 24 h) in DMF. Peptide cleavage from the resin was performed using a mixture of 88% trifluoroacetic acid (TFA), 5% phenol, 5% deionized H_2O and 2% triisopropyl silane (TIPS) (10 ml for 1 g of resin). The reaction ran for 2 h at ambient temperature. After 2 h the solution was filtered from the resin, concentrated under vacuum and treated with ice-cold Et_2O to precipitate the peptide. The precipitated peptides were centrifuged for 15 min at 4000 rpm at 4°C, the Et_2O phase was decantated (this step was repeated three times). Crude peptides were dissolved in deionized H_2O and lyophilized.

4.5. Peptide purification

Linear peptides and peptides with disulphide bridges were dissolved in AcOH and adjusted with deionized H_2O to an AcOH concentration of 10%. Peptides with nonprotected cysteine residues were dissolved in H_2O with addition of a 10-fold excess of dithiothreitol (DTT) and kept in an ultrasonic bath at 60 °C for 30 min. Crude peptides were purified using RP-HPLC technique on a semi-preparative Luna C8 (2) (250 mm × 20 mm, 5 μm) column from Phenomenex (Torrance, CA, USA). The mobile phase used during peptide purification consisted of (A) 0.01 M ammonium acetate in deionized H_2O and (B) 60% (v:v) acetonitrile (ACN) in deionized H_2O containing 0.01 M ammonium acetate. A linear gradient from 20 to 30% B to 50–60% B over 80 min. was applied for peptides containing more than 10 amino acid residues and from 5% B to 30% B over 100 min. for short peptides. The separation process was monitored by UV absorbance at 223 and 254 nm. Peptide purity was confirmed by (i) RP-HPLC using a Kromasil C8 (250 mm × 4.6 mm, 5 μm) analytical column, using a linear gradient from 5 % B to 100% B over 60 min, where (A) was 0.1% (v:v) TFA in deionized H_2O and (B) was 80% ACN in H_2O containing 0.08% (v:v) TFA, and (ii) liquid chromatography coupled with electrospray ionization, ion trap, and time-of-flight mass spectroscopy (LC ESI-IT-TOF MS) (Shimadzu, Shimpol, Warsaw, Poland).

4.6. Formation of disulphide bonds

In order to create disulphide bonds, each peptide with a free/unprotected sulfhydryl group in its cysteine residues was dissolved in a solution of H_2O:MeOH:AcOH (1:9:1, v:v:v) adjusted with iodine in MeOH (20–50-fold excess). The peptide concentration in the mixture was 40 mg/L. The reaction was conducted for 1 h at ambient temperature with constant stirring. The excess of iodine was removed by filtration of the solution through a Dowex ion exchange resin. In the next step, the solution was evaporated and the peptide lyophilized. The progress of the reaction was monitored by analytical RP-HPLC and LC ESI-IT-TOF MS (conditions provided above in the peptide purification section).

4.7. Binding assay - SPR analysis

Standard surface plasmon resonance analyses using Biacore T200 equipment (Cytiva, Malborough, USA) were performed as described in the manufacturer's manual. The interaction of PD-1 peptides with PD-L1 protein was analyzed using human His-PD-L1 protein (GenScript Biotech, New Jersey, USA, PD-L1 #Z03425) immobilized on a CM5 Sensor Chip (Cytiva, Malborough, USA) in a 10 mM sodium acetate buffer, pH 4.5, as described previously [46]. PD-L1 protein was immobilized to the 6500 RU ± 880 RU level of response. Serial dilutions of all peptides (Table 1) were prepared in PBS-P buffer (Cytiva, Malborough, USA #28995084) and injected over the prepared surface of a CM5 sensor chip. As a control, the binding of whole human PD-1 Fc Chimera protein (GenScript Biotech, New Jersey, USA, # Z03370) was analyzed. In all experiments PBS-P buffer was used as the running buffer. All analyses were performed at 25°C. The sensor chips surfaces were regenerated with 1.5 M NaCl and 10 mM glycine, pH 3. After each analysis an additional wash with 50% DMSO solution was performed. In all kinetics experiments, the buffer flow rate was set to 30 μl/min. The obtained data were analyzed using Biacore T200 Evaluation Software (Cytiva, Malborough, USA). The results are presented as sensorgrams obtained after subtraction of the background response signal from a reference flow cell

and from a control experiment with buffer injection. The kinetic constants of interaction between PD-L1 protein and selected peptides were calculated from at least three independent titration experiments, including at least two independent PD-L1 protein immobilizations. Kinetic constants were calculated for those peptides that showed interaction with PD-L1 protein.

4.8. Stability of peptides in RPMI 1640 medium

Peptide stability tests were performed in RPMI 1640 Medium (Sigma-Aldrich, #R8758) with 10% fetal bovine serum (FBS) (Thermo Fisher Scientific, #10500064). 200 µl of the RPMI 1640 was added to 50 µl of peptide, so the final concentration of peptide was 100 µM. The mixture was incubated at 37°C with constant stirring. Samples were collected at time 0 and after 24 h of incubation and immediately transferred to a freezer and stored until the end of the experiment at −80°C. The samples were thawed on ice. The peptides were precipitated by addition of a 4-fold excess of absolute ethanol (v:v) and centrifuged at 15,000 rpm for 20 min at 4°C. The supernatant was collected and evaporated. Dry samples were resuspended in 100 uL of 0.1% TFA in H_2O and analysed by analytical RP-HPLC using a Luna C18(2) (250 mm × 4.6 mm, 5 µm) analytical column under conditions described in the peptide purification section. All stability tests were performed at least in triplicate. Two control tests were performed in parallel to checking the influence of the test procedure on the peptide dissolved in water (without the medium and FBS) and on the medium (without the peptide).

4.9. Viability assay in Jurkat E6.1 and CHO-K1 cells

The viability of mammalian cells (as assessed by ATP) exposed to the synthesised peptides was tested in Jurkat E6.1 and CHO-K1 cell lines. CHO-K1 cells were seeded 24 h prior to the experiment on 96-well white plates at a density of 10,000 cells/well and incubated at 37°C in an atmosphere of 5% CO_2. On the day of the assay, a 3-fold serial dilution of the peptides in HAM-12 medium with 10% FBS was prepared (Merck, #N6658 and Thermo Fisher Scientific, #10500064, respectively). The final concentrations of peptides ranged from 150 µM to 0.62 µM. The diluted peptides were added to the wells with CHO-K1 cells, from which the medium had been removed shortly beforehand, and incubated for a further 24 h. Jurkat E6.1 cells were seeded on white 96-well plates, on the day of experiment, at a density of 20,000 cells/well. A 3-fold serial dilution of the peptides were prepared in RPMI-1640 medium (Sigma-Aldrich, #R8758) with 10% FBS and added to the Jurkat E6.1 cells, then incubated for 24 h under standard cell culture conditions. The final concentrations of peptide ranged from 150 µM to 0.62 µM. Before the final step the plates were equilibrated at ambient temperature for 10 min. CellTiter-Glo® (Promega Corporation, Madison, WI, USA, #G7570) was subsequently added to each well and incubated for 15 min. The luminescence was measured using a Spark M10 (Tecan, Switzerland) reader, with integration time 0.5 s. The data were analysed by GraphPad Prism 8 software.

4.10. Bioluminescent cell-based PD-1/PD-L1 immune checkpoint blockade assay

The inhibition potency of the peptides was examined using a PD-1/PD-L1 blockade bioassay kit (Promega Corporation, Madison, WI, USA, #J1250). The tests were performed according to the manufacturer's protocol. aAPC/CHO-K1 cells expressing PD-L1 protein were seeded 17 h prior to the experiments on 96-well white plates, at a density of 10,000 cells/well, and incubated at 37°C in an atmosphere of 5% CO_2. On the day of the assay, 3-fold serial dilutions of the peptides in assay buffer (RPMI 1640 with 1% FBS) were prepared. The final concentrations of the peptides ranged from 50 µM to 0.62 µM. Anti-PD-1 Ab (Promega Corporation, Madison, WI, USA (#J1201) was used as a positive control and prepared in the assay buffer at 10-fold dilutions. The diluted peptides and Ab were added to the wells seeded with aAPC/CHO-K1 cells, from which the medium had been removed shortly beforehand, and incubated for 1.5 h. Effector Jurkat E6.1 cells expressing PD-1 and NFAT-RE-induced luciferase were subsequently added at a density of 20,000 cells/well and incubated for 6 h under the aforementioned conditions. Before the final step the plates were equilibrated at ambient temperature for 10 min. In the next stage of the test, Bio-Glo™ Luciferase Assay reagent was added to each well and incubated for 15 min. The luminescence was measured with a Spark M10 (Tecan, Switzerland) reader, integration time 0.5 s. Data were analysed by GraphPad Prism 8 software.

4.11. NMR measurements

The NMR experiments were conducted at 298 K on a Bruker Avance III 500 MHz (^{1}H frequency 500.13 MHz) machine operated at magnetic fields of 11.7 T. The initial concentration of the sample was 6.4 mM in H_2O/D_2O (v:v; 9:1). The following NMR experiments were recorded: 1D 1H, 80 ms TOCSY, 300 ms ROESY, 200 ms NOESY and ^{1}H–^{13}C HSQC. The 2D heteronuclear spectrum was recorded on the natural abundance of ^{13}C isotope. All chemical shifts were referenced with respect to external sodium 2,2-dimethyl-2-silapentane-5-sulfonate (DSS) using $\Xi = 0.251449530$ ratio for indirectly referenced ^{13}C resonances [73].

4.12. NMR structure calculations

Molecular dynamics simulations were carried out using the ff14SB force field in the AMBER 16 package [66]. The structures of the peptides were computed using a simulated annealing algorithm with interproton distance restraints. The interproton distances were calculated on the basis of NOEs intensities by the CALIBA algorithm of the CYANA 2.1 program [74]. Simulated annealing started from a random conformation. The interproton distances were restrained with force constants of f = 50 kcal/(mol × Å^2). The geometry of the peptide groups (all trans) was kept fixed according to the NMR data (f = 50 kcal/(mol × rad^2)). 300 simulated annealing cycles were carried out where the nth conformation initiated the n + 1 cycle. Each simulated annealing cycle consisted of 30,000 MD steps (30 ps). The system was heated for 1 ps to 1200 K, annealed at 1200 K for 2 ps, and finally cooled to 0 K over 27 ps. A generalized Born model was used to approximate solvent interaction [75]. The structures were subsequently minimized without any constraints. The conformations within a relative energy cut-off of 20 kcal/mol, with respect to the lowest energy conformation, were selected for further analysis. The set of conformations was then clustered into conformational families using the Hierarchical agglomerative algorithm implemented in the CPPTRAJ module of the AMBER 16 package. Visualization of the structures was achieved with the aid of the VMD program [71].

4.13. Docking of the PD-1 derived peptides to PD-L1

Molecular docking of the peptides **(10)** and **(4)** to PD-L1 was performed with an UNRES force field [76,77], using multiplexed-replica exchange molecular dynamics with weak restraints on the torsional and valence angles of the backbone and weak restraints on the side chain–side chain and peptide group–peptide group contacts based on the crystal structure of PD-1/PD-L1 [78].

$$V_x = -\sum_i ln\left\{\sum_{m=1}^{M} exp\left[-1/2\left(\frac{x_i - x_i^{(m)}}{\sigma_{xi}^{(m)}}\right)\right]\right\}$$

where Vx is the restraint potential, xi is distance or angle and the $xi^{(m)}$ is the value of the template, σ is the variance of the potential. Each restraint is multiplied by appropriate weight.

For distance restraints (side-chain – side-chain and peptide group

peptide group) weight was set to 0.02 kcal/mol while for local restrains weight was set to 0.5 kcal/mol. The sigma for distance restraints was set to 0.5 Å while for local retrain sigma was set to 0.1 rad. In addition, in the case of peptide **(10)**, two variants of restraints were used based on the NMR family structures of the monomers obtained from the NMR experiment. It should be noted that no restraints were imposed on the protein–protein interface. There were 20 starting structures, each consisting of two molecules randomly oriented with respect to each other. The temperatures 250, 260, 270, 280, 285, 290, 295, 300, 305, 310, 315, 320, 330, 340, 350, 360, 370, 380, 390, and 400 K, with two trajectories per temperature, were used. Each simulation comprised 10,000,000 steps with a time step of 0.49 fs, which corresponds to 5 ns of UNRES time, which in turn corresponds approximately to 5 μs of real-time [79,80]. Subsequently, a bin-less weighted histogram analysis method (WHAM) was performed, along with clustering at a temperature of 300 K to obtain 10 clusters for each simulation. The cluster representative structure was the one closest to the ensemble average. The RMSD of the structures were computed for Cα atoms with use of the trimmed crystal as reference.

4.14. Determination of the kinetic constants of PD-1 derived peptides to PD-L1

UNRES force field canonical molecular dynamics was performed to determine the association/dissociation rate constant and equilibrium dissociation constant. As in the previous simulations 20 randomly structures were used and weak restraints, as in the MREMD simulations, were imposed. To obtain good statistics 100 canonical molecular dynamics simulations for peptide **(10)** were performed with a Berendsen thermostat at 300 K. In the case of peptide **(4)** 300 trajectories were run to obtain sufficient statistics. From the trajectories the fraction of properly unbound peptide as a function of time was computed and the kinetic equation derived previously was used [81].

Funding

This work was financially supported by the Polpharma Scientific Foundation under Grant No. 1/XVIII/19.

CRediT authorship contribution statement

Magdalena Bojko: Methodology, Validation, Formal analysis, Investigation, Writing – original draft, Visualization. **Katarzyna Węgrzyn:** Methodology, Validation, Formal analysis, Investigation, Visualization. **Emilia Sikorska:** Methodology, Software, Validation, Formal analysis, Investigation, Visualization. **Mikołaj Kocikowski:** Methodology, Investigation. **Maciej Parys:** Investigation. **Claire Battin:** Methodology, Investigation. **Peter Steinberger:** Methodology, Investigation. **Małgorzata M. Kogut:** Methodology, Software, Validation, Formal analysis, Investigation, Visualization. **Michał Winnicki:** Investigation. **Adam K. Sieradzan:** Methodology, Software, Validation, Formal analysis, Investigation, Visualization. **Marta Spodzieja:** Conceptualization, Methodology, Investigation, Writing – original draft, Supervision. **Sylwia Rodziewicz-Motowidło:** Conceptualization, Supervision, Project administration, Funding acquisition.

Declaration of Competing Interest

The authors declare that they have no known competing financial interests or personal relationships that could have appeared to influence the work reported in this paper.

Data availability

Data will be made available on request.

Appendix A. Supplementary material

Supplementary data to this article can be found online at https://doi.org/10.1016/j.bioorg.2022.106047.

References

[1] Y. Iwai, M. Ishida, Y. Tanaka, T. Okazaki, T. Honjo, N. Minato, Involvement of PD-L1 on tumor cells in the escape from host immune system and tumor immunotherapy by PD-L1 blockade, Proc. Natl. Acad. Sci. U. S. A. 99 (2002) 12293–12297, https://doi.org/10.1073/pnas.192461099.
[2] R.M. Poole, Pembrolizumab: First global approval, Drugs. 74 (2014) 1973–1981, https://doi.org/10.1007/s40265-014-0314-5.
[3] S.L. Topalian, M. Sznol, D.F. McDermott, H.M. Kluger, R.D. Carvajal, W. H. Sharfman, J.R. Brahmer, D.P. Lawrence, M.B. Atkins, J.D. Powderly, P. D. Leming, E.J. Lipson, I. Puzanov, D.C. Smith, J.M. Taube, J.M. Wigginton, G. D. Kollia, A. Gupta, D.M. Pardoll, J.A. Sosman, F.S. Hodi, Survival, durable tumor remission, and long-term safety in patients with advanced melanoma receiving nivolumab, J. Clin. Oncol. 32 (2014) 1020–1030, https://doi.org/10.1200/JCO.2013.53.0105.
[4] R. Gentzler, R. Hall, P.R. Kunk, E. Gaughan, P. Dillon, C.L. Slingluff, O.E. Rahma, Beyond melanoma: inhibiting the PD-1/PD-L1 pathway in solid tumors, Immunotherapy. 8 (5) (2016) 583–600.
[5] A. Markham, S. Duggan, Cemiplimab: First Global Approval, Drugs. 78 (17) (2018) 1841–1846.
[6] E.S. Kim, Avelumab: First Global Approval, Drugs. 77 (2017) 929–937, https://doi.org/10.1007/s40265-017-0749-6.
[7] Y.Y. Syed, Durvalumab: First Global Approval, Drugs. 77 (2017) 1369–1376, https://doi.org/10.1007/s40265-017-0782-5.
[8] A. Carretero-González, D. Lora, I. Ghanem, J. Zugazagoitia, D. Castellano, J. M. Sepúlveda, J.A. López-Martin, L. Paz-Ares, G. de Velasco, Analysis of response rate with ANTI PD1/PD-L1 monoclonal antibodies in advanced solid tumors: a meta-analysis of randomized clinical trials, Oncotarget. 9 (2018) 8706–8715, https://doi.org/10.18632/oncotarget.24283.
[9] Search of: mAb PD-L1 - List Results - ClinicalTrials.gov, (n.d.). https://www.clinicaltrials.gov/ct2/results?cond=&term=mAb+PD-L1&cntry=&state=&city=&dist= (accessed November 18, 2020).
[10] Search of: mAb PD-1 - List Results - ClinicalTrials.gov, (n.d.). https://www.clinicaltrials.gov/ct2/results?cond=&term=mAb+PD-1&cntry=&state=&city=&dist= (accessed November 18, 2020).
[11] Y. Ishida, Y. Agata, K. Shibahara, T. Honjo, Induced expression of PD-1, a novel member of the immunoglobulin gene superfamily, upon programmed cell death, accessed December 9, 2018, EMBO J. 11 (1992) 3887–3895, http://www.ncbi.nlm.nih.gov/pubmed/1396582.
[12] S. Tan, H. Zhang, Y. Chai, H. Song, Z. Tong, Q. Wang, J. Qi, G. Wong, X. Zhu, W. J. Liu, S. Gao, Z. Wang, Y. Shi, F. Yang, G.F. Gao, J. Yan, An unexpected N-terminal loop in PD-1 dominates binding by nivolumab, Nat. Commun. 8 (2017), https://doi.org/10.1038/ncomms14369.
[13] T. Okazaki, A. Maeda, H. Nishimura, T. Kurosaki, T. Honjo, PD-1 immunoreceptor inhibits B cell receptor-mediated signaling by recruiting src homology 2-domain-containing tyrosine phosphatase 2 to phosphotyrosine, Proc. Natl. Acad. Sci. U. S. A. 98 (2001) 13866–13871, https://doi.org/10.1073/pnas.231486598.
[14] S. Tang, P.S. Kim, A high-affinity human PD-1/PD-L2 complex informs avenues for small-molecule immune checkpoint drug discovery, Proc. Natl. Acad. Sci. 116 (2019) 24500–24506, https://doi.org/10.1073/pnas.1916916116.
[15] J.L. Riley, PD-1 signaling in primary T cells, Immunol. Rev. 229 (2009) 114–125, https://doi.org/10.1111/j.1600-065X.2009.00767.x.
[16] S.Y. Tseng, M. Otsuji, K. Gorski, X. Huang, J.E. Slansky, S.I. Pai, A. Shalabi, T. Shin, D.M. Pardoll, H. Tsuchiya, B7-DC, a new dendritic cell molecule with potent costimulatory properties for T cells, J. Exp. Med. 193 (2001) 839–845, https://doi.org/10.1084/jem.193.7.839.
[17] Y. Latchman, C.R. Wood, T. Chernova, D. Chaudhary, M. Borde, I. Chernova, Y. Iwai, A.J. Long, J.A. Brown, R. Nunes, E.A. Greenfield, K. Bourque, V. A. Boussiotis, L.L. Carter, B.M. Carreno, N. Malenkovich, H. Nishimura, T. Okazaki, T. Honjo, A.H. Sharpe, G.J. Freeman, PD-L2 is a second ligand for PD-1 and inhibits T cell activation, Nat. Immunol. 2 (2001) 261–268, https://doi.org/10.1038/85330.
[18] K. Pfistershammer, C. Klauser, W.F. Pickl, J. Stöckl, J. Leitner, G. Zlabinger, O. Majdic, P. Steinberger, No evidence for dualism in function and receptors: PD-L2/B7-DC is an inhibitory regulator of human T cell activation, Eur. J. Immunol. 36 (2006) 1104–1113, https://doi.org/10.1002/eji.200535344.
[19] L.M. Francisco, P.T. Sage, A.H. Sharpe, The PD-1 pathway in tolerance and autoimmunity, Immunol. Rev. 236 (2010) 219–242, https://doi.org/10.1111/j.1600-065X.2010.00923.x.
[20] N. Selenko-Gebauer, O. Majdic, A. Szekeres, G. Höfler, E. Guthann, U. Korthäuer, G. Zlabinger, P. Steinberger, W.F. Pickl, H. Stockinger, W. Knapp, J. Stöckl, B7–H1 (Programmed Death-1 Ligand) on Dendritic Cells Is Involved in the Induction and Maintenance of T Cell Anergy, J. Immunol. 170 (2003) 3637–3644, https://doi.org/10.4049/JIMMUNOL.170.7.3637.
[21] X. Wang, F. Teng, L. Kong, J. Yu, PD-L1 expression in human cancers and its association with clinical outcomes, Onco. Targets. Ther. 9 (2016) 5023–5039, https://doi.org/10.2147/OTT.S105862.

[22] T. Okazaki, T. Honjo, PD-1 and PD-1 ligands: From discovery to clinical application, Int. Immunol. 19 (2007) 813–824, https://doi.org/10.1093/intimm/dxm057.

[23] C. Solinas, A. Gombos, S. Latifyan, M. Piccart-Gebhart, M. Kok, L. Buisseret, Targeting immune checkpoints in breast cancer: an update of early results, ESMO Open. 2 (5) (2017) e000255, https://doi.org/10.1136/esmoopen-2017-000255.

[24] J.H. Yearley, C. Gibson, N. Yu, C. Moon, E. Murphy, J. Juco, J. Lunceford, J. Cheng, L.Q.M. Chow, T.Y. Seiwert, M. Handa, J.E. Tomassini, T. McClanahan, PD-L2 Expression in Human Tumors: Relevance to Anti-PD-1 Therapy in Cancer, Clin. Cancer Res. 23 (2017) 3158–3167. https://doi.org/10.1158/1078-0432.CCR-16-1761.

[25] X. Cheng, V. Veverka, A. Radhakrishnan, L.C. Waters, F.W. Muskett, S.H. Morgan, J. Huo, C. Yu, E.J. Evans, A.J. Leslie, M. Griffiths, C. Stubberfield, R. Griffin, A. J. Henry, A. Jansson, J.E. Ladbury, S. Ikemizu, M.D. Carr, S.J. Davis, Structure and interactions of the human programmed cell death 1 receptor, J. Biol. Chem. 288 (2013) 11771–11785, https://doi.org/10.1074/jbc.M112.448126.

[26] D.Y.W. Lin, Y. Tanaka, M. Iwasaki, A.G. Gittis, H.P. Su, B. Mikami, T. Okazaki, T. Honjo, N. Minato, D.N. Garboczi, The PD-1/PD-L1 complex resembles the antigen-binding Fv domains of antibodies and T cell receptors, Proc. Natl. Acad. Sci. U. S. A. 105 (2008) 3011–3016, https://doi.org/10.1073/pnas.0712278105.

[27] E. Lazar-Molnar, Q. Yan, E. Cao, U. Ramagopal, S.G. Nathenson, S.C. Almo, Crystal structure of the complex between programmed death-1 (PD-1) and its ligand PD-L2, Proc. Natl. Acad. Sci. 105 (2008) 10483–10488, https://doi.org/10.1073/pnas.0804453105.

[28] Q. Li, L. Quan, J. Lyu, Z. He, X. Wang, J. Meng, Z. Zhao, L. Zhu, X. Liu, H. Li, Discovery of peptide inhibitors targeting human programmed death 1 (PD-1) receptor, Oncotarget. 7 (40) (2016) 64967–64976.

[29] K.M. Zak, R. Kitel, S. Przetocka, P. Golik, K. Guzik, B. Musielak, A. Dömling, G. Dubin, T.A. Holak, Structure of the Complex of Human Programmed Death 1, PD-1, and Its Ligand PD-L1, Structure. 23 (2015) 2341–2348, https://doi.org/10.1016/j.str.2015.09.010.

[30] Y. Chen, P. Liu, F. Gao, H. Cheng, J. Qi, G.F. Gao, A dimeric structure of PD-L1: Functional units or evolutionary relics? Protein Cell. 1 (2010) 153–160, https://doi.org/10.1007/s13238-010-0022-1.

[31] K. Guzik, M. Tomala, D. Muszak, M. Konieczny, A. Hec, U. Błaszkiewicz, M. Pustuła, R. Butera, A. Dömling, T.A. Holak, K. Guzik, M. Tomala, D. Muszak, M. Konieczny, A. Hec, U. Błaszkiewicz, M. Pustuła, R. Butera, A. Dömling, T. A. Holak, Development of the Inhibitors That Target the PD-1/PD-L1 Interaction—A Brief Look at Progress on Small Molecules, Peptides and Macrocycles, Molecules 24 (2019) 2071, https://doi.org/10.3390/molecules24112071.

[32] N.G. Jørgensen, J. Kaae, J.H. Grauslund, Ö. Met, S.L. Nielsen, A.W. Pedersen, I. M. Svane, E. Ehrnrooth, M.H. Andersen, C. Zachariae, L. Skov, Vaccination against PD-L1 with IO103 a Novel Immune Modulatory Vaccine in Basal Cell Carcinoma: A Phase IIa Study, Cancers (Basel). 13 (2021) 911, https://doi.org/10.3390/cancers13040911.

[33] E. Zyla, B. Musielak, T.A. Holak, G. Dubin, Structural Characterization of a Macrocyclic Peptide Modulator of the PD-1/PD-L1 Immune Checkpoint Axis, Molecules. 26 (2021) 4848, https://doi.org/10.3390/molecules26164848.

[34] L.L. Chepelev, N.L. Chepelev, H. Shadnia, W.G. Willmore, J.S. Wright, M. Dumontier, Development of Small-Molecule Ligands and Inhibitors, Protein Target. Small Mol. Chem. Biol. Tech. Appl. (2009) 115–147, https://doi.org/10.1002/9780470495018.ch7.

[35] L. Nevola, E. Giralt, Modulating protein-protein interactions: The potential of peptides, Chem. Commun. 51 (2015) 3302–3315, https://doi.org/10.1039/c4cc08565e.

[36] J. Powderly, M.R. Patel, J.J. Lee, J. Brody, F. Meric-Bernstam, E. Hamilton, S. Ponce Aix, J. Garcia-Corbacho, Y.-J. Bang, M.-J. Ahn, S.Y. Rha, K.-P. Kim, M. Gil Martin, H. Wang, A. Lazorchak, T. Wyant, A. Ma, S. Agarwal, D. Tuck, A. Daud, CA-170, a first in class oral small molecule dual inhibitor of immune checkpoints PD-L1 and VISTA, demonstrates tumor growth inhibition in pre-clinical models and promotes T cell activation in Phase 1 study, Ann. Oncol. 28 (2017) v405–v406, https://doi.org/10.1093/annonc/mdx376.007.

[37] S.S.S.N. Pottayil Govindan Nair Sasikumar, Muralidhara Ramachandra, 1,3,4-Oxadiazole and 1,3,4-thiadiazole derivatives as immunomodulators, 2015.

[38] B. Musielak, J. Kocik, L. Skalniak, K. Magiera-Mularz, D. Sala, M. Czub, M. Stec, M. Siedlar, T.A. Holak, J. Plewka, CA-170 – A Potent Small-Molecule PD-L1 Inhibitor or Not? Molecules. 24 (2019) 2804, https://doi.org/10.3390/molecules24152804.

[39] D. Huang, W. Wen, X. Liu, Y. Li, J.Z.H. Zhang, Computational analysis of hot spots and binding mechanism in the PD-1/PD-L1 interaction, RSC Adv. 9 (2019) 14944–14956, https://doi.org/10.1039/c9ra01369e.

[40] H. Ding, H. Liu, Mapping the Binding Hot Spots on Human Programmed Cell Death 1 and Its Ligand with Free-Energy Simulations, J. Chem. Inf. Model. 59 (2019) 4339–4349, https://doi.org/10.1021/acs.jcim.9b00337.

[41] J. Du, Y. Qin, Y. Wu, W. Zhao, W. Zhai, Y. Qi, C. Wang, Y. Gao, The design of high affinity human PD-1 mutants by using molecular dynamics simulations (MD), Cell Commun. Signal. 16 (2018) 1–16, https://doi.org/10.1186/s12964-018-0239-9.

[42] K. Wang, Y. Song, Y. Su, Y. Liang, L. Wang, Effect of the hairpin structure of peptide inhibitors on the blockade of PD-1/PD-L1 axis, Biochem. Biophys. Res. Commun. 527 (2020) 453–457, https://doi.org/10.1016/j.bbrc.2020.04.018.

[43] W.-J. Jeong, J. Bu, Y. Han, A.J. Drelich, A. Nair, P. Král, S. Hong, Nanoparticle Conjugation Stabilizes and Multimerizes β-Hairpin Peptides to Effectively Target PD-1/PD-L1 β-Sheet-Rich Interfaces, J. Am. Chem. Soc. 142 (4) (2020) 1832–1837.

[44] K. Zhou, J.i. Lu, X. Yin, H. Xu, L. Li, B. Ma, Structure-based derivation and intramolecular cyclization of peptide inhibitors from PD-1/PD-L1 complex interface as immune checkpoint blockade for breast cancer immunotherapy, Biophys. Chem. 253 (2019) 106213.

[45] A. Ganesan, M. Ahmed, I. Okoye, E. Arutyunova, D. Babu, W.L. Turnbull, J. K. Kundu, J. Shields, K.C. Agopsowicz, L. Xu, Y. Tabana, N. Srivastava, G. Zhang, T. C. Moon, A. Belovodskiy, M. Hena, A.S. Kandadai, S.N. Hosseini, M. Hitt, J. Walker, M. Smylie, F.G. West, A.G. Siraki, M.J. Lemieux, S. Elahi, J.A. Nieman, D.L. Tyrrell, M. Houghton, K. Barakat, Comprehensive in vitro characterization of PD-L1 small molecule inhibitors, Sci. Rep. 9 (2019) 12392, https://doi.org/10.1038/s41598-019-48826-6.

[46] H.-N. Chang, B. Liu, Y. Qi, Y. Zhou, Y.-P. Chen, K.-M. Pan, W.-W. Li, X.-M. Zhou, W.-W. Ma, C.-Y. Fu, Y.-M. Qi, L. Liu, Y.-F. Gao, Blocking of the PD-1/PD-L1 Interaction by a <scp>D</scp> -Peptide Antagonist for Cancer Immunotherapy, Angew. Chemie Int. Ed. 54 (2015) 11760–11764, https://doi.org/10.1002/anie.201506225.

[47] V. Kotraiah, T.W. Phares, C.D. Browne, J. Pannucci, M. Mansour, A.R. Noe, K. D. Tucker, J.M. Christen, C. Reed, A. MacKay, G.M. Weir, R. Rajagopalan, M. M. Stanford, C.-S. Chung, A. Ayala, J. Huang, M. Tsuji, G.M. Gutierrez, Novel Peptide-Based PD1 Immunomodulators Demonstrate Efficacy in Infectious Disease Vaccines and Therapeutics, Front. Immunol. 11 (2020) 264, https://doi.org/10.3389/fimmu.2020.00264.

[48] K.L. Zapadka, F.J. Becher, A.L. Gomes dos Santos, S.E. Jackson, Factors affecting the physical stability (aggregation) of peptide therapeutics, Interface Focus. 7 (2017) 20170030, https://doi.org/10.1098/rsfs.2017.0030.

[49] L.H. Long, A. Hoi, B. Halliwell, Instability of, and generation of hydrogen peroxide by, phenolic compounds in cell culture media, Arch. Biochem. Biophys. 501 (2010) 162–169, https://doi.org/10.1016/j.abb.2010.06.012.

[50] L. Hua Long, B. Halliwell, Oxidation and Generation of Hydrogen Peroxide by Thiol Compounds in Commonly Used Cell Culture Media, Biochem. Biophys. Res. Commun. 286 (5) (2001) 991–994.

[51] K. Kuncewicz, C. Battin, A. Sieradzan, A. Karczyńska, M. Orlikowska, A. Wardowska, M. Pikuła, P. Steinberger, S. Rodziewicz-Motowidło, M. Spodzieja, Fragments of gd protein as inhibitors of btla/hvem complex formation—design, synthesis, and cellular studies, Int. J. Mol. Sci. 21 (2020) 1–19, https://doi.org/10.3390/ijms21228876.

[52] T. Riss, D. Ph, Cell Titer -G LO ^{TM} luminescent cell viability assay: A sensitive and rapid method for determining cell, n.d., 11–13.

[53] K. Magiera-Mularz, K. Kuska, L. Skalniak, P. Grudnik, B. Musielak, J. Plewka, J. Kocik, M. Stec, K. Weglarczyk, D. Sala, B. Wladyka, M. Siedlar, T.A. Holak, G. Dubin, Macrocyclic Peptide Inhibitor of PD-1/PD-L1 Immune Checkpoint, Adv. Ther. 4 (2021) 2000195, https://doi.org/10.1002/adtp.202000195.

[54] K. Magiera-Mularz, L. Skalniak, K.M. Zak, B. Musielak, E. Rudzinska-Szostak, Ł. Berlicki, J. Kocik, P. Grudnik, D. Sala, T. Zarganes-Tzitzikas, S. Shaabani, A. Dömling, G. Dubin, T.A. Holak, Bioactive Macrocyclic Inhibitors of the PD-1/PD-L1 Immune Checkpoint, Angew. Chemie - Int. Ed. 56 (2017) 13732–13735, https://doi.org/10.1002/anie.201707707.

[55] R.J. Boohaker, V. Sambandam, I. Segura, J. Miller, M. Suto, B. Xu, Rational design and development of a peptide inhibitor for the PD-1/PD-L1 interaction, Cancer Lett. 434 (2018) 11–21, https://doi.org/10.1016/j.canlet.2018.04.031.

[56] H. Liu, Z. Zhao, L. Zhang, Y. Li, A. Jain, A. Barve, W. Jin, Y. Liu, J. Fetse, K. Cheng, Discovery of low-molecular weight anti-PD-L1 peptides for cancer immunotherapy, J. Immunother. Cancer. 7 (2019) 270, https://doi.org/10.1186/s40425-019-0705-y.

[57] A. Riccio, A. Coletti, D. Dolciami, A. Mammoli, B. Cerra, S. Moretti, A. Gioiello, S. Ferlin, E. Puxeddu, A. Macchiarulo, The Stone Guest: How Does pH Affect Binding Properties of PD-1/PD-L1 Inhibitors? ChemMedChem. 16 (2021) 568–577, https://doi.org/10.1002/cmdc.202000760.

[58] E. Jurrus, D. Engel, K. Star, K. Monson, J. Brandi, L.E. Felberg, D.H. Brookes, L. Wilson, J. Chen, K. Liles, M. Chun, P. Li, D.W. Gohara, T. Dolinsky, R. Konecny, D.R. Koes, J.E. Nielsen, T. Head-Gordon, W. Geng, R. Krasny, G. Wei, M.J. Holst, J. A. McCammon, N.A. Baker, Improvements to the <scp>APBS</scp> biomolecular solvation software suite, Protein Sci. 27 (2018) 112–128, https://doi.org/10.1002/pro.3280.

[59] N. Raghunand, X. He, R. van Sluis, B. Mahoney, B. Baggett, C.W. Taylor, G. Paine-Murrieta, D. Roe, Z.M. Bhujwalla, R.J. Gillies, Enhancement of chemotherapy by manipulation of tumour pH, Br. J. Cancer. 80 (1999) 1005–1011, https://doi.org/10.1038/sj.bjc.6690455.

[60] D.E. Korenchan, R.R. Flavell, Spatiotemporal pH Heterogeneity as a Promoter of Cancer Progression and Therapeutic Resistance, Cancers (Basel). 11 (2019) 1026, https://doi.org/10.3390/cancers11071026.

[61] J.E. Ippolito, M.W. Brandenburg, X. Ge, J.R. Crowley, K.M. Kirmess, A. Som, D. A. D'Avignon, J.M. Arbeit, S. Achilefu, K.E. Yarasheski, J. Milbrandt, M. Tan, Extracellular pH Modulates Neuroendocrine Prostate Cancer Cell Metabolism and Susceptibility to the Mitochondrial Inhibitor Niclosamide, PLoS One. 11 (7) (2016) e0159675, https://doi.org/10.1371/journal.pone.0159675.

[62] D.J. Craik, D.P. Fairlie, S. Liras, D. Price, The Future of Peptide-based Drugs, Chem. Biol. Drug Des. 81 (2013) 136–147, https://doi.org/10.1111/cbdd.12055.

[63] M. Pelay-Gimeno, A. Glas, O. Koch, T.N. Grossmann, Structure-Based Design of Inhibitors of Protein-Protein Interactions: Mimicking Peptide Binding Epitopes, Angew. Chemie - Int. Ed. 54 (2015) 8896–8927, https://doi.org/10.1002/anie.201412070.

[64] P. Vlieghe, V. Lisowski, J. Martinez, M. Khrestchatisky, Synthetic therapeutic peptides: science and market, Drug Discov. Today. 15 (2010) 40–56, https://doi.org/10.1016/J.DRUDIS.2009.10.009.

[65] P.G. Sasikumar, M. Ramachandra, Small-Molecule Immune Checkpoint Inhibitors Targeting PD-1/PD-L1 and Other Emerging Checkpoint Pathways, BioDrugs. 32 (2018) 481–497, https://doi.org/10.1007/s40259-018-0303-4.

[66] D.A. Case, R.M. Betz, D.S. Cerutti, C.I. T.E., T.A. Darden, R.E. Duke, T.J. Giese, H. Gohlke, A.W. Goetz, N. Homeyer, S. Izadi, P. Janowski, J. Kaus, A. Kovalenko, T.S. Lee, S. LeGrand, P. Li, C.Lin, T. Luchko, R. Luo, B. Madej, D. Mermelstein, K.M. Merz, G. Monard, H. Nguyen, H.T. Nguyen, I. Omelyan, A. Onufriev, D.R. Roe, A. Roitberg, C. Sagui, C.L. Simmerling, W.M. Botello-Smith, J. Swails, R.C. Walker, J. Wang, R.M. Wolf, X. Wu, L. Xiao, P.A. Kollman, Amber 2016, Univ. California, San Fr. (2016).

[67] J.A. Maier, C. Martinez, K. Kasavajhala, L. Wickstrom, K.E. Hauser, C. Simmerling, ff14SB: Improving the Accuracy of Protein Side Chain and Backbone Parameters from ff99SB, J. Chem. Theory Comput. 11 (2015) 3696–3713, https://doi.org/10.1021/acs.jctc.5b00255.

[68] V. Hornak, R. Abel, A. Okur, B. Strockbine, A. Roitberg, C. Simmerling, Comparison of multiple Amber force fields and development of improved protein backbone parameters, Proteins Struct. Funct. Bioinforma. 65 (2006) 712–725, https://doi.org/10.1002/prot.21123.

[69] V. Tsui, D.A. Case, Theory and Applications of the Generalized Born Solvation Model in Macromolecular Simulations, Biopolymers. 56 (4) (2000) 275–291.

[70] A. Onufriev, D. Bashford, D.A. Case, Modification of the Generalized Born Model Suitable for Macromolecules, J. Phys. Chem. B. 104 (2002) 3712–3720, https://doi.org/10.1021/jp994072s.

[71] W. Humphrey, A. Dalke, K. Schulten, VMD: Visual molecular dynamics, J. Mol. Graph. 14 (1996) 33–38, https://doi.org/10.1016/0263-7855(96)00018-5.

[72] D.R. Roe, T.E. Cheatham, PTRAJ and CPPTRAJ: Software for Processing and Analysis of Molecular Dynamics Trajectory Data, J. Chem. Theory Comput. 9 (7) (2013) 3084–3095.

[73] D.S. Wishart, C.G. Bigam, J. Yao, F. Abildgaard, H.J. Dyson, E. Oldfield, J. L. Markley, B.D. Sykes, 1H, 13C and 15N chemical shift referencing in biomolecular NMR, J. Biomol. NMR. 6 (2) (1995) 135–140.

[74] P. Güntert, C. Mumenthaler, K. Wüthrich, Torsion angle dynamics for protein structure calculations with a new program, DYANA, J. Mol. Biol. 273 (1997) 283–298.

[75] H. Nguyen, D.R. Roe, C. Simmerling, Improved generalized born solvent model parameters for protein simulations, J. Chem. Theory Comput. 9 (2013) 2020–2034, https://doi.org/10.1021/ct3010485.

[76] A.K. Sieradzan, Introduction of periodic boundary conditions into UNRES force field, J. Comput. Chem. 36 (2015) 940–946, https://doi.org/10.1002/jcc.23864.

[77] A.K. Sieradzan, P. Krupa, H.A. Scheraga, A. Liwo, C. Czaplewski, Physics-based potentials for the coupling between backbone- and side-chain-local conformational states in the United Residue (UNRES) force field for protein simulations, J. Chem. Theory Comput. 11 (2015) 817–831, https://doi.org/10.1021/ct500736a.

[78] A. Karczyńska, M.A. Mozolewska, P. Krupa, A. Giełdoń, K.K. Bojarski, B. Zaborowski, A. Liwo, R. Ślusarz, M. Ślusarz, J. Lee, K. Joo, C. Czaplewski, Use of the UNRES force field in template-assisted prediction of protein structures and the refinement of server models: Test with CASP12 targets, J. Mol. Graph. Model. 83 (2018) 92–99, https://doi.org/10.1016/j.jmgm.2018.05.008.

[79] M. Khalili, A. Liwo, A. Jagielska, H.A. Scheraga, Molecular Dynamics with the United-Residue Model of Polypeptide Chains. II. Langevin and Berendsen-Bath Dynamics and Tests on Model <img src="http://pubs.acs.org/images/gifchars/alpha.gif" border="0">-Helical Systems, J. Phys. Chem. B. 109 (2005) 13798–13810.

[80] A. Liwo, M. Khalili, H.A. Scheraga, Ab initio simulations of protein-folding pathways by molecular dynamics with the united-residue model of polypeptide chains, Proc. Natl. Acad. Sci. 102 (2005) 2362–2367, https://doi.org/10.1073/pnas.0408885102.

[81] M. Spodzieja, K. Kuncewicz, A. Sieradzan, A. Karczyńska, J. Iwaszkiewicz, V. Cesson, K. Węgrzyn, I. Zhukov, M. Maszota-Zieleniak, O. Michielin, D.E. Speiser, V. Zoete, L. Derré, S. Rodziewicz-Motowidło, Disulfide-Linked Peptides for Blocking BTLA/HVEM Binding, Int. J. Mol. Sci. 21 (2020) 636, https://doi.org/10.3390/ijms21020636.